

PROPOSAL FOR A NEW NEUTRINO DETECTOR AT FERMILAB

P. Berge, D. Bogert, J. Griffin, R. Hanft,
M. Johnson, P. Limon, T. Ohsugi, F. Nezrick,
L. Stutte, J. K. Walker,* and J. Wolfson
Fermi National Accelerator Laboratory
Batavia, Illinois 60510

and

F. E. Taylor*
Northern Illinois University
DeKalb, Illinois 60115

and

M. Block, D. Buchholz, B. Gobbi,
and D. Miller*
Northwestern University
Evanston, Illinois 60201

* Principal Investigators

97 pgs.

ABSTRACT

We propose a massive 500 ton neutrino detector for Fermilab which provides detailed information on final-state electrons, muons, and hadrons. The detector can be triggered selectively; its good sensitivity allows exploration of a new range of physics inaccessible to present bubble chambers and electronic detectors. The design is based on plastic flash tubes, a tenth-scale prototype of which we have tested successfully. Results from these tests demonstrate that:

- a) both energy and angle can be measured with good resolution for electrons up to 40 GeV; and b) angular resolution for hadronic energy flow is near the theoretical limit set by shower fluctuations.

The detector is modular, technically straightforward to construct, and inexpensive. We estimate that we can begin taking data one year from date of approval. Recording and interpreting the data inevitably involve complex problems in pattern recognition which must be addressed manually. The Film Analysis Facility at Fermilab is ideally suited to perform this function. The semi-automatic device, SAMM, is well matched to scanning and measuring the film.

We request rapid approval to proceed with construction of the detector. In addition, we request an initial run in 1978 with the new dichromatic beam; the principal emphasis in this data run would be the study of neutral current interactions and production of multilepton final states including electrons.

CONTENTS

- I. Introduction
- II. Physics Justification
- III. Detector
 - A. General Description - Flash Chambers
 - B. Proportional Tubes
 - C. Scintillation Counters
 - D. Detector Tests
 - E. Large Scale Prototype Flash Chamber Production
 - F. Data Acquisition
- IV. Detector Characteristics
- V. Semi-Leptonic Neutral Current Reaction
- VI. Four Fermion Reaction
- VII. Rates
- VIII. Costs, Time Schedule and Requests
- Appendix A. Detector Tests
- Appendix B. Engineering Design Study of 500 Ton Target Fabrication
(Summary of Neutrino Lab Report)

I. INTRODUCTION

Recent experiments on the interaction of high energy neutrinos have provided clear evidence that the weak interactions remain a rich and exciting area for future investigations. Among the most dramatic discoveries are:

1) The existence of neutral currents.¹ To study this reaction further it is necessary to explore both its Lorentz structure and internal symmetries. The first step constitutes accurate measurements in the scaling variables x and y .

2) Events involving the production of two or more leptons.² The observation of enhanced strangeness production in di-lepton events is consistent with production of charmed particles. However, the unexpectedly large muon momenta observed in tri-muon final states suggests a new source of leptons.

3) Anomalous behavior at high y in antineutrino interactions.³ If verified, this could signal the existence of new quarks with right-handed couplings to neutrinos.

Thus far, it has been possible to carry out these studies only with muon-type neutrinos. It is apparent that these observations are reflections from the tips of only the highest mountains to be explored. A systematic study is now essential at the next level of sensitivity with both muon- and electron-neutrinos.

To carry out such a program we have designed a massive detector whose major new features include:

a) measurement of hadronic energy flow, both direction and total energy.

b) electron identification, with measurement of both the direction and total energy of the associated shower.

To provide the necessary muon identification and momentum measurement we propose that the detector be installed upstream of the existing toroids in Lab C. The total mass of the detector is 500 tons. The fiducial volume will be determined by cuts depending on the reaction studied. Production rates for particular final states are optimized by choice of neutrino beam and selective triggering. The sensitivity and versatility of the detector, which combines several features of separate visual and electronic detectors, are crucial to further investigation of a variety of neutrino-induced final states:

1) The narrow-band neutrino beam provides neutrinos of well-defined energies. A measurement of hadronic energy flow then allows a detailed mapping of neutral current interactions in the scaling variables x and y . Such data provide an initial confrontation with numerous theoretical models.

2) Since high energy neutrinos from K-decay are enhanced, relative to neutrinos from π -decay, the narrow-band beam is also well suited to the study of multilepton final states. A measurement of hadronic energy flow for events with 3μ , $2\mu + e$, etc. provides an estimate of transverse momentum imbalance. A large imbalance would indicate an energetic decay involving neutrinos.

The proposed detector is technically straight-forward, economical, and represents a major advance in Fermilab's ability to confront the most challenging aspects of high energy neutrino interactions. Since construction is modular the detector can be increased to 3000 tons or changed to another configuration as progress in physics dictates. There is no other detector existing or planned at CERN SPS or Fermilab which can address the same range of physics.

II. PHYSICS JUSTIFICATION

The mass of the proposed detector is comparable to that of existing detectors at Fermilab and CERN. Hence, the justification for the new detector must lie in the new qualitative features of the data to be obtained. These features are electron identification, and hadron energy flow. We will briefly discuss some of the general questions on which the new data will shed light.

1. Semi-leptonic Neutral Current Reactions

The reactions of interest are

$$\nu_{\mu} (\bar{\nu}_{\mu}) + N \rightarrow \nu_{\mu} (\bar{\nu}_{\mu}) + \text{hadrons.} \quad (1)$$

The major objective of this experiment is to study the energy and angular distribution of these neutral current reactions up to 350 GeV neutrino energy. Neither of the Fermilab electronic neutrino detectors has the necessary angular resolution to perform this study. The results will reveal the space-time structure of the hadronic weak neutral current and its symmetry properties.

Knowledge of the energy and direction of the incident neutrino is essential to this experiment. This is achieved with the new 350 GeV dichromatic beam. The hadron total energy, E_H , and direction, θ_H , of energy flow are measured in a ≥ 300 ton fiducial weight detector. We have measured the angular resolution for θ_H (see Appendix A for details); it is close to the theoretical limit set by fluctuations in the hadronic cascade. Hence a detailed study will be made of the distribution of events in q^2 and v , or correspondingly in the scaling variables $y = v/E_{\nu}$

and $x = q^2/2M\nu$. Clear event signature will be achieved by demanding the absence of a muon of energy greater than 2 GeV in the event. A typical event rate from K neutrinos is one per 30 pulses of 1.5×10^{13} protons with the narrow band beam set at 250 GeV.

Charged current data will be taken simultaneously with the neutral current data. Not only do the charged current events provide a continuous check of the apparatus but they provide additional information on possible high-y anomalies in $\bar{\nu}$ reactions.

2. Multi-lepton Production

Multi-muon events of unusual type, $\mu^{\pm}\mu^{\pm}$ and $\mu^{\pm}\mu^{\mp}\mu^{\pm}$ (and possibly 4 and 5 muon events) have recently been observed² at Fermilab. There are some indications³ that these reactions have a common origin since $\mu^{\pm}\mu^{\mp}$ correlations are similar in the two sets of events. We assume that the systematics of these processes will be explored in detail both at Fermilab and at CERN in the next year.

A qualitative increase in our understanding of this new physics would occur by observing the production of electrons in association with multimuons. It has been observed⁴ that the ratio of events of the type μe relative to regular charged current events is: $\mu e/\mu \approx 1\%$. This is probably too low a signal to successfully identify μe type events from background. However, as the ratio $\mu\mu\mu/\mu\mu$ appears⁵ to be more like 5-10% at $E_{\nu} > 100$ GeV, we expect to be able to identify $\mu\mu e$ type events if they occur with similar frequency. The rate may be higher, as, a priori one might expect the fraction $\frac{\mu\mu e}{\mu}$ to be twice the

fraction $\frac{\mu\mu\mu}{\mu} \approx 10-20\%$. The data we will obtain on multi-lepton events will be a strong constraint on possible production mechanisms.

The three-muon data shown in Fig. 1^b exhibit high transverse momenta of the muons. It is important to find out whether this transverse momentum is balanced by hadrons and if so, in what way. Alternatively, imbalance of transverse momentum would signal the presence of neutrinos. The proposed detector can measure the hadron transverse momentum with an accuracy of about 1 GeV/c.

Use of the narrow band beam to study multi-lepton production will allow a search for threshold behavior and missing energy in the form of neutrinos in the final state.

3. Neutrino Electron Elastic Scattering

The reactions of interest are:

$$\nu_e + e^- \rightarrow \nu_e + e^- \quad (2)$$

$$\bar{\nu}_e + e^- \rightarrow \bar{\nu}_e + e^- \quad (3)$$

$$\nu_\mu + e^- \rightarrow \nu_\mu + e^- \quad (4)$$

$$\bar{\nu}_\mu + e^- \rightarrow \bar{\nu}_\mu + e^- \quad (5)$$

The ν_e scattering can proceed via both charged and neutral current terms and will be an excellent way to study the CC-NC interference. We shall probably reserve this pleasure for the detector to one of the first uses of neutrinos from 1000 GeV protons.

The $(\bar{\nu})_{\mu}$ scattering can proceed only through the neutral current and provides a sensitive test of different gauge models without the complication of hadronic structure.

For energies $E_{\mu} > m_{\mu}^2/2m_e = 11 \text{ GeV}$ the reactions:

$$\nu_{\mu} + e^{-} \rightarrow \mu^{-} + \nu_e \quad (6)$$

$$\bar{\nu}_e + e^{-} \rightarrow \mu^{-} + \bar{\nu}_{\mu} \quad (7)$$

can be studied. These reactions are different forms of the inverse muon decay and involve the charged current only.

Reactions (4), (5) and (6) can be studied immediately with the detector and existing neutrino beams. A search for the reaction

$$\bar{\nu}_{\mu} + e^{-} \rightarrow \mu^{-} + \bar{\nu}_e \quad (8)$$

which violates the additive lepton number conservation law would also be made. Existing tests⁷ on the allowable extent of a multiplicative law are very unrestrictive. Both the Gargamelle⁸ and Aachen-Padua⁹ groups have probably observed the elastic neutrino scattering process. Some progress will occur with BEBC and the Fermilab 15' exposures and the approved counter experiment¹⁰ aimed at this process at Fermilab. However, the field is extremely difficult and will benefit greatly from a 500 ton detector which has the sensitivity and resolution designed to investigate these processes.

4. Electron Neutrino Interactions

We propose a study of the deep inelastic scattering of electron neutrinos.

$$\nu_e (\bar{\nu}_e) + N \rightarrow e^{\mp} + "X" \quad (9)$$

On the basis of gauge-theory folk-lore ν_e and ν_μ should behave similarly; nevertheless, there is great importance in experimentally exploring the general properties of ν_e interactions. The apparent absence of parity-violating neutral-current effects in atomic physics¹¹ suggests that there may be surprises for specific gauge-model advocates.

The ν_e beam^{2b} which we propose to use has equal numbers of ν_e and $\bar{\nu}_e$. As the detector cannot distinguish e^- from e^+ , we will measure the sum of the two charged current (cc) reactions:

$$\begin{aligned} \frac{d\sigma}{dx dy} (\nu_e + Z \rightarrow e^- + X) + \frac{d\sigma}{dx dy} (\bar{\nu}_e + Z \rightarrow e^+ + X) \\ = S_{\nu_e \bar{\nu}_e}^{cc} (x, y) \end{aligned} \quad (10)$$

This quantity $S_{\nu_e \bar{\nu}_e}^{cc}$ will be compared with the similarly averaged quantity $S_{\nu_\mu \bar{\nu}_\mu}^{cc}$ bin by bin as a function of q^2 and ν . Similar results should be obtained for the neutral current (nc) reactions and a comparison of $S_{\nu_e \bar{\nu}_e}^{nc}$ with $S_{\nu_\mu \bar{\nu}_\mu}^{nc}$ will be made.

Of course, in the neutral current data an approximate 50% background of events from neutral current interactions from ν_μ and $\bar{\nu}_\mu$ in the ν_e beam will have to be subtracted to obtain the final data. The question of the universality of ν_e and ν_μ neutral current interactions is a challenging one and we will be able to address this problem.

5. Beam Dump Study of New Forms of Neutrino

There is some evidence from SPEAR^{1,2} and DORIS^{1,3} that new heavy charged leptons of a flavor different from the conventional electron and muon type may be produced. They may or may not be associated with charm. Presumably, new associated neutrinos would exist as well. Although a conventional calculation of charm production in a beam dump and subsequent leptonic decay or Drell-Yan production of heavy leptons produce a disappointingly low flux of "heavy" neutrinos, ν_H say, there may be other more copious mechanisms of ν_H production.

We therefore propose a beam dump experiment to search for anomalous interactions in the detector which cannot be explained in any conventional way.

We believe our detector is ideally suited to this kind of experiment. In the search for new leptonic effects it is crucial to have:

- a) both electron and muon identification
- b) gamma ray detection capability
- c) ability to detect transverse momentum imbalance including the hadronic component to signify prompt neutrino emission

- d) fine granularity to look for long-lived neutral leptons decaying downstream of the vertex (a la Kolar Gold Field events)
- e) 500 ton mass for good sensitivity.

We would place a high priority on this search for the unexpected.

6. Neutrino Oscillations

Although there are no compelling theoretical arguments which suggest that there should be a finite mass associated with neutrinos it is an interesting experimental question. Recent intense experimental interest in lepton non-conservation in the $\mu \rightarrow e + \gamma$ process lends support to a study of oscillations of ν_μ into ν_e .

We propose using the booster cycling at 1.5 GeV/c during a period when the main ring is shut down due to power limitations, Energy Doubler/Saver installation or excavation for colliding beam experimental areas. Figure 2 shows a possible layout of a 70 foot long neutrino beam line in the tunnel leading from the booster to the transfer gallery. The beam is directed at Lab C. Use of a low energy beam allows greater sensitivity at large proper times $\tau = \ell/p$ (where ℓ is the flight length and p is the momentum of the neutrino). In addition, the low momentum permits use of a very pure ν_μ beam and allows kinematic suppression of all background reactions.

The oscillation $\nu_\mu \rightarrow \nu_e$ is detected by observation of the reaction



The products $e^- + p$ are observed in the 500 ton detector which is 3 km from the neutrino source. As the sensitivity to a neutrino mass scale enters in the ratio ℓ/p the use of 200 MeV neutrinos over 3 km is equivalent in this respect to the use of 40 GeV neutrinos over 600 km. An ultimate sensitivity of this experiment to a mass difference term of the order of 10^{-2} eV will be achieved.

Although, it is doubtful that we would propose constructing the detector for this experiment as a primary objective it appears reasonable with minimum additional investment to perform this interesting measurement.

III. DETECTOR

A. General Description

The neutrino target is to be used in conjunction with the large toroidal magnetic facility in Lab C at Fermilab. The target must have the following characteristics:

- a) Large mass (we will have ~ 500 tons).
- b) Fine grain sampling of event for hadronic energy flow measurements.
- c) Selective trigger.
- d) Ability to identify single and multiple electrons with good angular resolution.

- e) Ability to separate electromagnetic from hadronic cascades.
- f) Modular construction allowing reconfiguration in response to new physics results.
- g) Modest cost.

The proposed detector is shown in Fig. 3. The detector is 19.5 m long and has a hexagonal cross section with a 4.3 meter transverse size. The detector is located immediately upstream of the existing 24 feet diameter iron toroids in Lab C. Flash chambers¹⁴ are alternated with 3/8" thick sheets of fiber-reinforced cement and aluminum throughout the length of the detector. A sub-module is shown in Fig. 4 and a full module in Fig. 5. Optical information from the chamber is recorded directly on film and/or magnetic tape using electro-optical techniques. The detector is triggered using liquid scintillation counters which are located at 30.4 cm intervals throughout the detector.

The flash chambers are constructed from extruded polypropylene plastic at a cost of \$1.50/sq. meter. The individual cells of the plastic are 5 mm x 4 mm cross section and are filled with the standard spark chamber gas of 90% Ne + 10% He. Gas manifolds are thermo-vacuum formed from Uvac plastic. The gap between electrodes is chosen to be 32 mm. All cement sheets are covered with aluminum foil to minimize the required high voltage. When an event of interest is detected by the scintillation counters a high voltage pulse of ~ 24 kV is applied across the gap, thereby causing a glow discharge in the tubes where the particles traversed the chambers. The cement planes are fairly similar to aluminum in regard to radiation length and

collision length but are considerably less expensive.

The neutrino target is built up of alternating flash chamber and cement layers. Each flash chamber plane is rotated by 60° from the previous flash chamber layer to give x-y-u coordinate measurements. A 0.6 cm sheet of lead and a liquid scintillation counter are placed at 30.4 cm intervals throughout the neutrino target. The lead sheet helps to discriminate hadrons from electrons.

The total number of collision lengths in the target is roughly 44, the total number of radiation lengths is roughly 170 and the total weight is 500 tons.

B. Proportional Tubes

Two proportional tube hodoscope detector planes will be installed in addition to the existing coarse grained scintillation hodoscopes in the 24' toroid (see Fig. 6). These tubes will be constructed from extruded aluminum in the form of 12' long 1" square sections. The tubes will be vertical in all cases and one row will be stacked on top of another to cover the full 24' height of the toroid. Each plane will have a total of 576 detectors giving a total of 1152 wires.

Each tube has a 50 μm diameter gold plated tungsten wire centered in the 1" x 1" hole (see Fig. 7). The filling gas mixture will be 80% argon and 20% methane which provides a high drift velocity. Our tests with a full scale 12' long detector of this form show that the output pulse from the tube occurs

< 160 nsec after the particle traverses the detector. Excellent pulse height response is obtained as shown in Fig. 7, which shows the spectrum obtained with Fe^{55} . As pulse height information is not required from the detector but rather the digital information corresponding to whether it has been struck by a muon we can have a cheap amplifier (< \$12) on each wire. These tubes will provide a trigger for di-muons.

C. Scintillation Counters

The scintillation counters are used in triggering the detector in the manner described elsewhere and in hadron calorimetry. Total pulse height corresponding to energy loss in the scintillator is required for this purpose.

Although the flash chamber detector provides a good measure of the total electromagnetic energy as well as the electromagnetic and hadronic energy flow directions, we would like to use the scintillation counters to provide a measurement for the total energy deposited in the detector. The counters allow sampling of electromagnetic and hadronic cascades at 2.6 radiation lengths and 0.7 collision lengths respectively. The latter figure is similar to the hadronic cascade sampling frequencies in other neutrino detectors. It is possible that the flash chambers will provide an independent measurement of the hadronic energy but this has not yet been tested.

In addition, we would like to have spatial information from the scintillation counters which will provide an independent measurement of the energy flow direction. Previous attempts to extract spatial information from large area scintillation counters have relied upon the relative amplitude of the light

pulses arriving at a small number of phototubes on the edge of the scintillator. This provides a measurement of the light absorption and therefore the path length between the track location through the counter and each photomultiplier. Although good short-term results can be had for spatial resolution by this method, it is difficult to obtain good long-term stability for two reasons. These are the requirements of extremely good relative gain stability of the phototubes and stable light attenuation of the scintillation counter relative to the light shifter bars. It has been found that small impurities (such as water coming through plexiglass) in the liquid scintillator can cause significant change in the light attenuation length. For these reasons we do not propose a technique which relies on the pulse heights of the phototubes to locate the particle trajectory.

The design of the proposed scintillation counters is shown in Fig. 8. The counter is fabricated from a horizontal stacked array of extruded triangular plexiglass tubes filled with liquid scintillator. Each tube is optically decoupled from its neighbors by a 1 mil Aluminum foil. Due to the cross section of each tube the counter maintains uniform efficiency across its area. Internally reflected light emerging from the end of each tube passes through an air gap before entering a wave length shifter bar which internally reflects light to four phototubes at the corners of the counter.

The unique feature of this counter design is that for any position struck on the counter the light path to each phototube is specified. Consequently, measurement of the relative timing

of the output pulses of the phototubes provides accurate spatial reconstruction of the event. This technique is independent of sagging of photomultiplier gain or impurities of the liquid scintillator. Measurements of spatial reconstruction accuracies on a single long plastic scintillator are shown in Fig. 9 and indicate that for the dimensions of the counter proposed here, $\sigma_x = \sigma_y \approx 3$ cm can be achieved.

We have started doing prototype studies using a counter of this design. Knowledge of only the neutrino event vertex position from the flash chambers can be used with the pulse height and position information from the scintillation counters to provide a useful backup approach to studying neutral currents or the hadronic energy flow in other processes.

D. Detector Tests

An extensive series of tests have been made with a prototype detector which is ~10% of the length of the final proposed neutrino detector. This length is adequate for measuring the key parameters:

- a) hadron energy flow angular resolution
- b) electron energy and angle resolution.

These tests have been performed in the M5 test beam in the Meson Laboratory. Although the beam was limited to $E \leq 40$ GeV this is adequate to study the response of the detector to electrons. Figure 10 shows the expected electron energy distributions from various reactions and demonstrates that 40 GeV is quite adequate for test purposes. A full description of the tests and results are given in Appendix A.

E. Large Scale Prototype Flash Chamber Production

We have constructed 8 large (12' x 5') prototype flash chambers. The 5' long gas manifolds were thermo-vacuum formed in the same way as for the small chambers. Ten gas manifolds were formed at one time on a single mold. The process took about 10 minutes to fabricate 10 manifolds. Vacuum bonds of the manifolds to the extruded plastic were just as successful as with the smaller test chambers described in Appendix A. Some of the structural properties of stacks of the 12' x 5' chambers were investigated and we are confident that the proposed 4.3 m x 4.3 m chambers can be fabricated in the way described in the engineering design report issued by the Neutrino Department. Figure 11 shows a stack of the 12' x 5' chambers.

F. Data Acquisition

The flash tube detector will have on the order of 1 million tubes. We have investigated the possibility of electronic readout and we have confirmed the Conversi claim¹⁴ that signals of a volt across 50 Ω can be obtained directly from a probe inserted into the plasma. A data acquisition system involving a million wires is formidable but not out of the question and we are following both that approach and the alternative approach of optical read-out.

We are investigating the cost effectiveness of several alternative systems. One of these is recording the data on film with a mirror system similar to the one that exists for E-310. With

three cameras, each camera would view approximately 330,000 tubes of 5 mm on a side. Since E-310 has spatial resolution on this order, film will clearly work. It also should be no problem to measure the film on SAMM. With one event per two pulses, we would generate two rolls/day which should take SAMM one day to measure. This is certainly reasonable.

There is also the possibility of using an all electronic method of reading out the data. We are beginning to examine the possibility of using a solid state camera, either CCD (charge coupled device) or CID (charge injection device). One can buy units that have 250 x 250 cells (62,000 total) that readout in 1/30 of a second. One expects that a 512 x 512 array (250,000 elements) will be available shortly since this corresponds to the 525 line scan format of commercial television. Using conventional lenses, they have adequate resolution to readout the 5 mm tubes.

Processing 250,000 points/camera is somewhat of a problem. Since most of them are zero, a brute force method using a fast ECL preprocessor seems possible (250,000 points in 1/30 of a second is 100 ns/pt.) Perhaps a more elegant approach is using a CID device which can read-out individual cells similar to MOS computer memory.

An alternative approach is to use conventional vidicon tubes in a manner similar to that used successfully in previous large detectors such as the Omega spectrometer at CERN. The relative advantages of these systems are being examined at this time.

A reasonable way to proceed is to utilize film with its well understood technical aspects and make use of SAMM in the

Film Analysis Facility. As the detector begins to take larger quantities of data more automatic data recording could be implemented. However, the field of electro-optical recording is changing rapidly and we shall make our decision on data readout after an extensive review of the options.

IV. DETECTOR CHARACTERISTICS

A summary of the properties of the detector is given in Table I.

TABLE I
NEUTRINO TARGET PROPERTIES

Total Mass	500 tons
Fiducial Mass (Neutral Currents)	300 tons
Dimensions:	4.3 m x 4.3 m x 19 m
Location:	Lab C
Construction:	Layers of flash chambers giving 3 views sandwiched between layers of cement. Every 18 flash chamber planes there is 5 mm of Pb followed by a scintillation counter hodoscope.
Average density:	1.59 g/cm ³
Calorimeter properties:	Collision length: 43.4 cm Radiation length: 11.7 cm Sampling every 3.9% of collision length Sampling every 14% of radiation length (including lead plate) every 7% of radiation length otherwise.
Resolutions:	Vertex position: ± 2.5 mm Electron energy: $\frac{\Delta(E_e)}{E_e} \approx \pm 10\%$ for $5 \leq E_e \leq 40$ GeV

-21-

Electron polar angle: $\sigma(\theta_e) = 5 \text{ mrad}$

Hadron energy:
by use of
scintillation
counters $\frac{\sigma(E_H)}{E_H} = \pm 60\%/\sqrt{E_H}$

Hadron energy flow:
(Polar angle)

$$\sigma(\theta_H) = 8.0 + (520/E_H) \text{ mrad}$$

Muon momentum: $\frac{\Delta(P_\mu)}{P_\mu} = \pm 15\%$

Event handling:

1 event/1 msec horn pulse

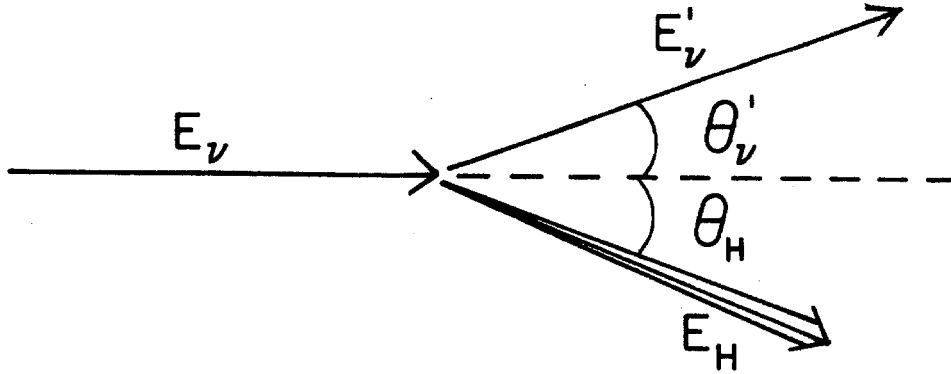
V. SEMI-LEPTONIC NEUTRAL CURRENT REACTIONS

The proposed detector is well suited for the measurement of the x and y structure of semi-leptonic neutral currents. The detector has the following characteristics relevant to this reaction; 1) large fiducial mass (≥ 300 tons) and hence high event rates in the narrow band beam, 2) good muon identification using the fine grain sampling flash chambers and the iron toroid facility 3) accurate measurement capability of the primary vertex position (thereby increasing the y acceptance and aiding in the determination of the narrow band beam energy), and 4) accurate measurement capability of the hadron energy flow (both energy and flow direction) using the flash chambers and scintillation counters.

To measure the semi-leptonic neutral current process, we must determine a) the kinematical acceptance, and b) the resolutions in the scaling variables x and y . We shall also discuss rates, expected backgrounds, and a trigger selective to neutral currents.

a) Kinematic Acceptance

The kinematics of the semi-leptonic neutral current reaction is specified by the incident neutrino energy E_ν (known a priori from the narrow band beam), the incident neutrino direction, the hadron energy E_H , and the hadron energy flow direction. These kinematic quantities are defined in the diagram.



It is of interest to study the neutral current cross section $d\sigma/dx dy$, in terms of the scaling variables x and y ; where

$$x = \frac{Q^2}{2m\nu}, \quad Q^2 = 4E_\nu E'_\nu \sin^2 \frac{\theta'_\nu}{2}, \quad \nu = E_H - M \quad (12)$$

$$y = (E_H - M)/E_\nu, \quad M = 0.94 \text{ GeV}/c^2. \quad (13)$$

The appropriate kinematics for the Fermilab narrow band beam^{1,5} for neutrinos and antineutrinos are shown in figures 12a and 12b respectively. From these kinematics we see that for $y_{\min} = 0.1$ the hadron energy ranges from 20 GeV to 250 GeV and the hadron energy flow direction ranges from 0° to 16° . Both of these ranges lie within the acceptance of the detector.

The acceptance in y is from 0.1 to 0.9. The lower limit of y is chosen to select only K-neutrino events. This discrimination is accomplished by measuring the radial position of the primary vertex and using the different angle-energy correlations of the K neutrinos and the π neutrinos in the narrow band beam.

The neutrino energy and the corresponding y_{\min} versus the radial distance from the center of the neutrino beam is shown in Fig. 13a and Fig. 13b respectively and for the antineutrino beam in Fig. 13c and 13d respectively. (The finite secondary beam phase space has not been included in these figures.) We see that a detector radius of 1.8 m at approximately 1.2 km from the meson decay corresponds to $y_{\min} \approx 0.1$ for both the neutrino and the antineutrino beam. The acceptance in y becomes flat above $y = 0.45$, since for $y > 0.45$ no radius cut is necessary to eliminate π -neutrino events. The discrimination against charge current events requires some minimum detectable energy left to the muon (or electron) in the final state. Hence $y_{\max} = 0.9$ implying $E_{\mu}(\min) = 14$ GeV and is therefore easily detectable.

The acceptance in x ranges from $0. \leq x \leq 1.0$, however some inefficiency of the detector occurs at small y -large x where the hadron angle becomes large with respect to the incident neutrino direction. Since these low y events must be detected at a large radius to discriminate against π -neutrino events, some fraction of the hadron shower can sometimes escape the detector.

These considerations were included in a Monte Carlo program which computed the acceptance of the detector for unambiguous neutral current events as a function of x and y . A neutral current "event" at a given x and y was accepted if: a) the primary vertex was at a radial distance from the neutrino beam axis satisfying $R_{\min} \leq R_v \leq 1.8$ m, where we approximate the relations in Fig. 3b and 4b by $R_{\min} = (0.44 - y)/0.23$ meters, b) the

lepton traveled 20λ (λ = collision length in the detector = 43.4 cm). (This was required since wide angle charge current events could be confused with neutral current events), and c) the hadron shower could flow 15λ in the detector.

The maximum radius of the detector was assumed to be 2.0 m. The results of this calculation are shown in Tables II and III for a positive secondary energy of 250 GeV and a negative secondary energy of 200 GeV respectively. The acceptance is generally $> 80\%$ over the table except for low y , or large x . The inefficiency at low y is due to the radius cut, required for π -neutrino discrimination and the inefficiency at large x is due to large angles of either the lepton or hadrons.

b) Resolution Function

The resolutions in x and y are computed by folding in the neutrino beam energy resolution, the angular resolution of the hadron energy flow (See Appendix A for the details of the measurement of this resolution), and the hadron energy resolution.

The narrow band beam resolution with the primary vertex measured by the flash chambers is assumed to be $\sigma(E_\nu) = 0.059 \sqrt{E_\nu}$. The resolution in the hadron energy flow direction (polar angle) is given by $\sigma(\theta_H) = 0.008 + 0.520/E_H$ (E_H in GeV). This is determined from the measured projected angular resolution from the M5 beam tests.

TABLE II
ACCEPTANCE FOR K-NEUTRINOS

$$E_K^+ = 250 \text{ GeV}$$

$x \backslash y$	0.1	0.3	0.5	0.7	0.9
0.1	0.248	0.172	0.151	0.149	0.140
0.3	0.864	0.803	0.711	0.671	0.651
0.5	0.991	0.921	0.842	0.794	0.745
0.7	0.963	0.890	0.782	0.719	0.686
0.9	0.842	0.653	0.551	0.433	0.351

Average acceptance = 0.629

TABLE III
ACCEPTANCE FOR K-ANTINEUTRINOS

$$E_K^- = 200 \text{ GeV}$$

$x \backslash y$	0.1	0.3	0.5	0.7	0.9
0.1	0.227	0.160	0.145	0.141	0.123
0.3	0.860	0.777	0.669	0.629	0.599
0.5	0.986	0.893	0.803	0.740	0.694
0.7	0.950	0.861	0.752	0.678	0.630
0.9	0.814	0.617	0.478	0.356	0.274

Average acceptance = 0.549

The hadron energy is measured by using the scintillation counters which sample the hadronic shower every 0.7 of a collision length and every 2.6 of a radiation length. The resolution of the hadron energy is estimated to be $\sigma(E_H) = 0.6 \sqrt{E_H}$ (E_H in GeV) from linearly scaling the resolution of a CITF calorimeter^{1b} which sampled the hadron shower every collision length in iron to the proposed calorimeter which will sample the hadron shower every 0.7 of a collision length. In addition the flash chamber information may be used to measure the hadron energy by counting the number of cells which fire as is done for measuring electron energies. The resolution obtainable however, by this method for hadron showers is at present unknown.

A Monte Carlo program was written which reconstructed measurable neutral current events at secondary beam energies of $E^+ = 250$ GeV and $E^- = 200$ GeV with the experimental uncertainties described above. The results are shown in Table IV and V for K-neutrinos in the dichromatic beam. It is noticed that the error in y is determined by the error in E_ν for $E_H \geq 50$ GeV, and for $E_H < 50$ GeV, has roughly equal contributions from the errors in the incident neutrino energy and in the hadron energy. The error in x depends on all the measured quantities E_ν , E_H , and θ_H and hence is correspondingly larger.

TABLE IV
RESOLUTIONS
 $E_{K^+} = 250 \text{ GeV}$

$x \backslash y$	0.1	0.3	0.5	0.7	0.9
0.1	0.07 / 0.012	0.13 / 0.013	0.16 / 0.013	0.20 / 0.015	0.25 / 0.014
0.3	0.07 / 0.029	0.13 / 0.028	0.17 / 0.027	0.21 / 0.027	0.23 / 0.028
0.5	0.09 / 0.04	0.17 / 0.04	0.21 / 0.04	0.27 / 0.04	0.29 / 0.04
0.7	0.15 / 0.05	0.24 / 0.05	0.31 / 0.05	0.45 / 0.06	0.51 / 0.05
0.9	0.64 / 0.06	1.02 / 0.07	1.3 / 0.06	1.6 / 0.07	1.5 / 0.06

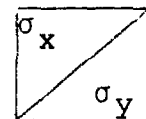
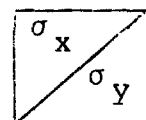


TABLE V
RESOLUTIONS
 $E_{K^-} = 200 \text{ GeV}$

$x \backslash y$	0.1	0.3	0.5	0.7	0.9
0.1	0.08 / 0.014	0.13 / 0.015	0.17 / 0.014	0.21 / 0.016	0.27 / 0.016
0.3	0.07 / 0.03	0.13 / 0.03	0.18 / 0.03	0.21 / 0.03	0.24 / 0.03
0.5	0.09 / 0.04	0.16 / 0.04	0.21 / 0.04	0.26 / 0.04	0.29 / 0.04
0.7	0.14 / 0.06	0.24 / 0.05	0.30 / 0.05	0.42 / 0.06	0.52 / 0.06
0.9	0.61 / 0.07	0.94 / 0.07	1.26 / 0.07	1.4 / 0.07	1.4 / 0.07



c) Event Rates

The neutral current event rates are computed by assuming:

$$\frac{d\sigma}{dx dy} \nu, \bar{\nu} \text{ (NC)} = \frac{d\sigma}{dx dy} \nu, \bar{\nu} \text{ (CC)} \frac{\sigma \text{ (NC)}}{\sigma \text{ (CC)}} \quad (14)$$

where we take:¹⁷

$$\frac{d\sigma}{dx dy} \nu N \text{ (CC)} = \frac{G^2 M E_\nu}{\pi} F_2 \nu N(x) \quad (15)$$

$$\frac{d\sigma}{dx dy} \bar{\nu} N \text{ (CC)} = \frac{G^2 M E_\nu}{\pi} F_2 \bar{\nu} N(x) (1-y)^2 \quad (16)$$

We shall approximate: $F_2^{\nu N}(x) = F_2^{\bar{\nu} N}(x) = \frac{1}{1.8} F_2^{\text{ed}}(x)$ measured at SLAC.¹⁸ We assume

$$\frac{\sigma^{\nu N} \text{ (NC)}}{\sigma^{\nu N} \text{ (CC)}} = 0.2 \text{ and } \frac{\sigma^{\bar{\nu} N} \text{ (NC)}}{\sigma^{\bar{\nu} N} \text{ (CC)}} = 0.4 \quad (17)$$

The target fiducial mass is 300 tons with a fiducial cross section of 10 m^2 corresponding to 1.8×10^{32} nucleons or 1.8×10^{27} nucleons/cm² presented to the narrow band beam. The incident neutrino flux is determined by the new "twisted beam" version of the narrow band beam.¹⁵ It is assumed that the neutrino and antineutrino flux is uniform over the fiducial area of 10 m^2 of the detector. The rates are calculated for 6×10^{18} protons on target for both neutrino and antineutrino exposures. The secondary beam momentum is set at 250 GeV/c for

neutrinos and at 200 GeV/c for neutrinos.

Putting all these factors together we have: (for kaon-neutrinos)

$$\frac{dN^{\nu N} \text{ events}}{dx dy} = 36000 F_2^{\nu N}(x) \quad (18)$$

$$\frac{dN^{\bar{\nu} N} \text{ events}}{dx dy} = 7000 F_2^{\nu N}(x) (1-y)^2 \quad (19)$$

Folding in the acceptance with these differential rates, we find the rates (in bins $\Delta X = 0.2$ and $\Delta y = 0.2$) given in Tables VI and VII. The rates are for K-neutrino component of the narrow band beam.

We note that for the neutrino exposure, it is possible to measure out to $x = 0.8$. For the antineutrino exposure, data may be taken out to $x = 0.6$. Increased statistics for antineutrinos may be obtained by running the secondary momentum at 100 GeV instead of 200 GeV. The K^- rates in the secondary beam would be increased by a factor of 5. We shall measure the neutrino induced neutral currents first and judging from our experience, select an appropriate antineutrino beam energy.

TABLE VI
 K^+ -NEUTRINO EVENTS FOR $E_{K^+} = 250$ GeV

$y \backslash x$	0.1±0.1	0.3±0.1	0.5±0.1	0.7±0.1	0.9±0.1
0.1 ± 0.1	438	216	64	10.4	0.4
0.3 ± 0.1	1528	1008	300	46.8	1.4
0.5 ± 0.1	1752	1156	356	55.2	1.8
0.7 ± 0.1	1702	1118	232	50.0	1.6
0.9 ± 0.1	1488	820	234	30.2	0.8

$\Sigma = 12710$ events

TABLE VII
 K^- -ANTINEUTRINO EVENTS FOR $E_{K^-} = 200$ GeV

$y \backslash x$	0.1±0.1	0.3±0.1	0.5±0.1	0.7±0.1	0.9±0.1
0.1 ± 0.1	63.2	31.6	9.6	2.0	0.04
0.3 ± 0.1	144.8	93.0	27.0	4.2	0.12
0.5 ± 0.1	84.8	54.6	16.4	2.6	0.06
0.7 ± 0.1	29.4	19.0	5.6	0.8	0.02
0.9 ± 0.1	2.8	2.0	0.4	0.04	0.002

$\Sigma = 592$ events

d) Backgrounds

Background events in the measurement of neutral currents have several sources. There can be cosmic ray events with an incident neutral particle which can mimic a neutral current event. These events may be reduced by using a short beam spill and by mixing a known sample of cosmic ray events with neutrino events by triggering the detector during the accelerator off time. The background due to misidentified charge current events is more serious. The $y < 0.9$ cut requires that the charge current event muon must have $E_{\mu} > 14$ GeV. The monitoring of charge current events allows a subtraction of this background by extrapolating the charge current rates into the kinematic region where charge current events become ambiguous with neutral currents.

The background from the wide band neutrinos in the narrow band beam is small. From the design report of the twisted narrow band beam,¹⁵ this background is $< 6\%$ for both neutrino and anti-neutrino beams. A measurement of this background may be made by taking data with the secondary beam slits closed.

e) Trigger

To trigger on neutral currents we require a local energy deposition of > 10 GeV together with a veto at the back of the 24 foot toroids and a veto at the front of the detector. Experience with the two existing neutrino detectors has shown that this trigger is adequate to keep the trigger rate to less than one trigger per millisecond of pulse. Another trigger will be used to simultaneously record charge current events.

VI. THE FOUR FERMION REACTION $\nu_e e^- \rightarrow \nu_\mu e^-$

One of the most fundamental reactions which can be studied in neutrino physics is the pure leptonic neutrino elastic scattering. Several major difficulties must be overcome in this study. They include: a) low event rate requiring a large mass detector and b) large backgrounds which necessitate a fine-grained high resolution detector. We shall first discuss background discrimination for the elastic neutrino-electron scattering reaction:

$$\nu_\mu e^- \rightarrow \nu_\mu e^- \tag{20}$$

There exist two important sources of background, the quasi-elastic inverse beta-decay of the neutron

$$\nu_e n \rightarrow p e^- \tag{21}$$

and single π^0 production by the neutral current neutrino interaction

$$\nu_\mu N \rightarrow \nu_\mu N \pi^0 \tag{22}$$

Both background reactions are dominated by nucleon form factors with masses $\sim m_p$ and tend to constant cross sections of

$$\sigma(\nu_e n \rightarrow pe^-) = 10^{-38} \text{ cm}^2 \quad (23)$$

$$\sigma(\nu_\mu N \rightarrow \nu_\mu N\pi^0) = 2 \cdot 10^{-39} \text{ cm}^2. \quad (24)$$

Background Due to $\nu_e n \rightarrow pe^-$

Electrons from elastic $\nu_e e$ scattering (20) are peaked in a forward cone of angle $\theta_e = \sqrt{\frac{2m_e}{E_\nu}}$ where E_ν is the energy of the incoming neutrino. They are therefore confined to small transverse momenta, $p_\perp \lesssim 200 \text{ MeV}/c$. Electrons from the inverse beta-decay process (21) have a much broader p_\perp distribution, with a mean value of $\bar{p}_\perp \approx \sqrt{Q^2} \approx 500 \text{ MeV}/c$. Thus it seems feasible to discriminate between the two reactions using a cut in p_\perp .

Figure 14 shows the expected number of events for $\nu_e e$ elastic scattering and inverse beta-decay as a function of p_\perp . To obtain these distributions, the following assumptions were made:

- 1) 2×10^{13} protons/pulse at 400 GeV
 12 second cycle time
 1000 hours of running
 i.e. 6×10^{18} protons on target
- 2) The two-horn system neutrino beam¹⁹
- 3) $\nu_e/\nu_\mu = 1\%$
- 4) A 360 ton fiducial volume in this detector.

For $\nu_\mu e^- \rightarrow \nu_\mu e^-$

1) A Weinberg angle of $\sin^2 \theta_W = 0.35$

(i.e. $\sigma \approx 10^{-42} E_\nu \text{ cm}^2$)

2) The functional form ²⁰

$$\frac{d\sigma^{\nu, \bar{\nu}}}{dE_e} = \frac{G^2 m_e}{2\pi E_\nu^2} \left[E_\nu^2 (g_V \pm g_A)^2 + (E_\nu - E_e)^2 (g_V \mp g_A)^2 + m_e E_e (g_A^2 - g_V^2) \right] \quad (25)$$

where $g_V = -1/2 + 2\sin^2 \theta_W$

$g_A = -1/2$

For $\begin{cases} \nu_e n \rightarrow p e^- \\ \bar{\nu}_e p \rightarrow n e^+ \end{cases}$

1. the functional form ²¹

$$\frac{d\sigma^{\nu, \bar{\nu}}}{dE_e} = \frac{M^3 G^2 \cos^2 \theta}{4\pi E_\nu^2} \left[A \mp B \frac{(S-U)}{M^2} + C \frac{(S-U)^2}{M^4} \right] \quad (26)$$

where $S-U = 2M(E_\nu + E_e)$

$$A = \frac{Q^2}{4M^2} \left[\left(4 + \frac{Q^2}{M^2}\right) F_A^2 - \left(4 - \frac{Q^2}{M^2}\right) F_{V1}^2 + \frac{Q^2}{M^2} \left(1 - \frac{Q^2}{4M^2}\right) F_{V2}^2 + \frac{4Q^2}{m^2} F_{V1} F_{V2} \right]$$

$$B = \frac{Q^2}{M^2} F_A (F_{V1} + F_{V2})$$

$$C = \frac{1}{4} (F_A^2 + F_{V1}^2 + \frac{Q^2}{4M^2} F_{V2}^2)$$

and F_{V1} , F_{V2} and F_A are the usual dipole-formula nucleon form factors.

The total number of events expected is 372 for $\nu_\mu e^- \rightarrow \nu_\mu e^-$ and 797 for $\nu_e n \rightarrow p e^-$. A p_\perp cut of 160 MeV/c reduces these numbers to 336 and 46, respectively (14% background). (Since $p_\perp \approx \sqrt{2m_p T_p}$, this is equivalent to the restriction on the kinetic energy of the proton $T_p < 13.6$ MeV, roughly the energy necessary to penetrate one cm of cement.) In addition, it has been shown²² that when inverse beta-decay takes place on bound neutrons, there will be significant suppression of this background due to Pauli exclusion. This has been included in the Monte Carlo as a multiplicative factor

$$R(\vec{Q}) = \frac{3}{2} \frac{\vec{Q}}{2P_F} - \frac{1}{2} \left(\frac{\vec{Q}}{2P_F} \right)^3 \quad \vec{Q} < 2 P_F \quad (27)$$

$$= 1$$

$$\vec{Q} \geq 2 P_F$$

where
$$\vec{Q} = \sqrt{Q^2 \left(1 + \frac{Q^2}{4M^2} \right)}$$

$$\text{and } P_F = 0.266 \text{ GeV}/c$$

This low Q^2 suppression reduces the background to about 4% under the elastic peak.

As mentioned earlier, the experimental resolutions as determined in the test apparatus were $\frac{\Delta E}{E} = \pm 10\%$ and $\sigma(\theta_e) = 4.3$ mrad. The resolutions were incorporated into the above Monte Carlo studies.

The angular resolution obtained in the test apparatus is for a projected angle. The Monte Carlo calculation uses a polar angle, so that for the calculation the resolution was multiplied by $\sqrt{2}$.

In addition, in the final apparatus, the average radiation length is 11.7 cm, compared to 10 cm for the test apparatus, so that the resolution used was $\sigma(\theta_e) = 4.3 \times \sqrt{2} \times 10/11.7$
 $= 5$ mrads

The results are shown in figures 15 and 16. The electron energy spectra (Fig. 15) remain virtually the same.

The p_{\perp} distribution, (Fig. 16) therefore, was calculated incorporating only the angular resolution, since this is by far the dominant source of error.

This distribution has been smeared, but separation of the two processes is clearly possible. The background for a p_{\perp} cut of 160 MeV/c is estimated to be 12% and can be statistically subtracted by observing the inverse beta-decay rate at higher p_{\perp} and using the predicted curve to extrapolate to smaller p_{\perp} .

Background Due to $\nu_\mu N \rightarrow \nu_\mu N\pi^0$

This background is potentially much more serious than inverse beta-decay since the ν_μ flux is 100 times the ν_e flux. Assuming a cross section of $2 \times 10^{-39} \text{ cm}^2$, we estimate 38,400 events of this type. Because of the nucleon form factors, the hadron energies one expects are quite small ($< 5 \text{ GeV}$). Indeed, the $N\pi^0$ mass spectrum is dominated²³ by Δ (1232) production. One can express the energy of the Δ as

$$E_\Delta = \frac{M_\Delta^2 + m_N^2 + Q^2}{2m_N}, \quad (28)$$

so that the kinetic energy of the Δ is roughly the same as that of the proton in inverse beta-decay (Fig. 17). If one considers the worst case, i.e. the π^0 takes away the maximum possible energy, $E_{\pi^0} \approx E_\Delta - M_N$, then

$$E_{\pi^0} = \frac{M_\Delta^2 - M_N^2 + Q^2}{2M_N}. \quad (29)$$

If one makes a cut on observed electromagnetic energy $E > 5 \text{ GeV}$ then this restricts the above neutral current reaction to $Q^2 > 8.76 \text{ GeV}^2$. Assuming the usual quadratic form factor with $M = M_p$, this implies the neutral current events with $Q^2 > 8.76 \text{ GeV}^2$ are less than 0.1% of the total, i.e. about 30 background events remain. In addition, the p_\perp distribution of the

π^0 is quite spread out, so further rejection of this background is possible using angular criteria and by demanding no other hadrons be visible.

As further evidence that this background is well in hand, consider the results of a CERN group⁹ who studied the four-fermion process in a beam of average energy $\langle E_\nu \rangle = 1.5$ GeV with a detector of the same sampling frequency. Their background from $\nu_\mu N \rightarrow \nu_\mu N \pi^0$ was estimated to be $\approx 50\%$. The Fermilab two-horn beam has $\langle E_\nu \rangle = 35$ GeV. Since the four-fermion cross section rises linearly with energy, while $\sigma(\nu_\mu N \rightarrow \nu_\mu N \pi^0)$ is constant, estimated backgrounds from this process should only be a few percent.

Table VIII gives predictions of event rates and background employing the above cuts.

VII. EVENT RATES

The event rates for the first run on neutral currents have been discussed in detail earlier. In this section we give some rates for several other reactions with different beams.

The rates for several reactions and beams have been calculated for the detector described assuming

- (1) a fiducial area of 10.6 m^2 ,
- (2) the number of target nucleons is $1.83 \times 10^{27}/\text{cm}^2$ and the number of electrons is $8.6 \times 10^{26}/\text{cm}^2$, (300 tons)
- (3) a total of 6×10^{18} protons at 400 GeV.

Four different beams were considered in calculating the rates.

TABLE VIII

EVENTS EXPECTED

(Experimental Resolutions Included)

NEUTRINO RUNNING			
PROCESS	TOTAL	$P_{\perp} < 160 \text{ MeV}/c$	$E_e > 5 \text{ GeV}$
$\nu_{\mu} e^{-} \rightarrow \nu_{\mu} e^{-}$	372	290	193
$\bar{\nu}_{\mu} e^{-} \rightarrow \bar{\nu}_{\mu} e^{-}$	55	46	31
$\nu_e n \rightarrow p e^{-}$	797 (708) ⁺	65 (34) ⁺	48 (22) ⁺
$\bar{\nu}_e p \rightarrow n e^{+}$	53 (47) ⁺	4 (2) ⁺	3 (1) ⁺
$\nu_{\mu} N \rightarrow \nu_{\mu} N \pi^0$	38400	-	30 [*]
$\bar{\nu}_{\mu} N \rightarrow \bar{\nu}_{\mu} N \pi^0$	2550	-	2 [*]
ANTINEUTRINO RUNNING			
PROCESS	TOTAL	$P_{\perp} < 160 \text{ MeV}/c$	$E_e > 5 \text{ GeV}$
$\nu_{\mu} e^{-} \rightarrow \nu_{\mu} e^{-}$	75	58	39
$\bar{\nu}_{\mu} e^{-} \rightarrow \bar{\nu}_{\mu} e^{-}$	358	300	202
$\nu_e n \rightarrow p e^{-}$	114 (101) ⁺	9 (5) ⁺	7 (3) ⁺
$\bar{\nu}_e p \rightarrow n e^{+}$	460 (408) ⁺	35 (17) ⁺	26 (8) ⁺
$\nu_{\mu} N \rightarrow \nu_{\mu} N \pi^0$	5490	-	4 [*]
$\bar{\nu}_{\mu} N \rightarrow \bar{\nu}_{\mu} N \pi^0$	22130	-	17 [*]

* Further suppression is possible with additional cuts on angle, extra track present, etc.

⁺ Numbers in parentheses include estimates of the effect of Pauli exclusion.

The numbers of events were calculated using

$$\text{Yield} = NA \int \sigma(E_\nu) F(E_\nu) dE_\nu \quad (30)$$

where N is the number of target particles/area

A is the fiducial area

$\sigma(E_\nu)$ is the cross section as a function of energy
and $F(E_\nu)$ is the flux of neutrinos as a function of energy.

The assumed cross sections were the following:

(1) Elastic reactions

$$\sigma = \sigma_0 E_\nu (B^2 + 1/3C^2) \quad (31)$$

where

$$\sigma_0 = 0.42 \times 10^{-41} \text{ cm}^2/\text{GeV} \quad (32)$$

and B and C are constants of the order of 1 which depend on which theory is being used (V-A, Weinberg, Salam, etc.)

(2) Inverse muon β -decay

$$\sigma = G^2/\pi \frac{(s-m_\mu^2)^2}{s} \text{ for } E_\nu > E_{th} \quad (33)$$

where $s = 2m_e E_\nu$

and $E_{th} = \frac{m_\mu^2}{2m_e} = 10.9 \text{ GeV}$

(3) Deep inelastic reactions

$$\text{Charged current } \sigma_{\nu}^{\text{CC}} = (0.8 \times 10^{-38} \text{ cm}^2/\text{GeV}) E_{\nu} \quad (34)$$

$$\sigma_{\bar{\nu}}^{\text{CC}} = 1/3 \sigma_{\nu}^{\text{CC}} \quad (35)$$

$$\text{Neutral current } \sigma_{\nu}^{\text{NC}} = 0.25 \sigma_{\nu}^{\text{CC}} \quad (36)$$

$$\sigma_{\bar{\nu}}^{\text{NC}} = 0.4 \sigma_{\nu}^{\text{CC}} \quad (37)$$

TABLE IX

Theory Beam Reaction	V-A ν_e Beam	V-A Quad	V-A 2-horn	W-S x=.33 ν_e Beam	W-S x=.33 Quad	W-S x=.33 2-horn
<u>Elastic</u>						
$\nu_\mu e \rightarrow \nu_\mu e$	0	0	0	.3	92	380
$\bar{\nu}_\mu e \rightarrow \bar{\nu}_\mu e$	0	0	0	.5	23	177
$\bar{\nu}_e e \rightarrow \nu_e e$	13			9		
$\bar{\nu}_e e \rightarrow \bar{\nu}_e e$	4			4		
<u>μ-β decay</u>						
$\nu_\mu e^- \rightarrow \mu^- \nu_e$	2.4	1020	31,300			
<u>Deep inelastic</u>						
$\nu_e + N \rightarrow e^- + X$	5900					
$\bar{\nu}_e + N \rightarrow e^+ + X$	1970					
$\nu_e + N \rightarrow \nu_e + X$	1180					
$\bar{\nu}_e + N \rightarrow \bar{\nu}_e X$	790					
<u>Multilepton</u>						
$\nu_e + N \rightarrow e^+ e^- X$	60					
$\bar{\nu}_e + N \rightarrow e^+ e^- X$	20					
$\nu_\mu + N \rightarrow \mu^+ \mu^- X$		14,000	60,000			
$\nu_\mu + N \rightarrow \mu^- \mu^+ \mu^- X$			3,000			
$\nu_\mu + N \rightarrow \mu \mu e X$		140	6,000			
$\nu_\mu + N \rightarrow \mu \mu \mu X$		140	300			
$\nu_\mu + N \rightarrow 4\ell X$			2,400			

- (4) Multilepton production where ℓ stands for any charged lepton

$$\sigma_{\nu}^{2\ell} \approx 0.01 \sigma_{\nu}^{cc}$$

$$\sigma_{\nu}^{3\mu} \approx 5.10^{-4} \sigma_{\nu}^{cc} = 3 \sigma_{\nu}^{3\mu, e}$$

$$\sigma_{\nu}^{2\mu, e} \approx 10^{-3} \sigma_{\nu}^{cc} = 3 \sigma_{\nu}^{2\mu, e}$$

$$\sigma_{\nu}^{4\mu} \approx 5.10^{-5} \sigma_{\nu}^{cc} \quad (\text{based on one candidate in E-310})$$

$$\sigma_{\nu}^{4\ell} \approx 2^3 \sigma_{\nu}^{4\mu}$$

$$\approx 4.10^{-4} \sigma_{\nu}^{cc}$$

VIII. COSTS AND TIME SCHEDULE

The estimate of material cost for the detector is shown in Table X. The total cost of the detector is estimated to be \$600,000. Labor cost for the 500 ton detector fabrication has been estimated by the Neutrino Lab to be \$125,000. The construction of the flash chambers, driving high voltage electronics and film read-out can proceed immediately. No new technological developments are required. A preliminary engineering design study for production of the detector has been made by the Neutrino Lab staff, a summary of which is given in Appendix B.

The study shows that the complete detector would be operational 12 months from the time of approval. We request that Lab C be available in February 1978.

TABLE X

1.	<u>Flash Chambers</u>	
	485 ton detector (Appendix B)	
	172 submodules at \$2495 each	\$429,000
	High voltage electronics (The E-310 Marx generators will be used)	<u>\$ 20,000</u>
	Subtotal-	\$449,000
2.	<u>Scintillation Counters</u>	
	57 counters with light bars.	
	Liquid scintillator from E-310 will be used	\$ 21,000
	228 photomultipliers and bases (from E-310)	<u>\$(30,000)</u>
		\$ 21,000
3.	<u>Lead</u>	
	57 sheets (removed from E-310 gamma catchers)	(\$57,000)
4.	<u>Flash Chamber Read-Out System</u>	
	Lenses, mirrors (additional to E-310 mirrors)	\$30,000
5.	<u>Proportional Tube Detectors</u>	
	Extruded aluminum at \$1/lb.	\$ 6,000
	Wire mounting at \$3/wire	\$ 3,000
	Electronics at \$12/channel amp.	\$14,000
	Gas connections	<u>\$ 3,000</u>
		\$26,000

(continued on next page)

6. Miscellaneous

Gas circulation system	\$ 30,000
Fast electronics	<u>\$ 50,000</u>
Total	\$586,000

We request an initial run with the dichromatic beam starting in the summer of 1978. A possible set of runs is indicated in the Table below.

TABLE XI

<u>Incident Proton Energy</u> (GeV)	<u>Dichromatic Tune</u> (Polarity/GeV)	<u>No. of Protons</u>
400	+ 250	2×10^{18}
	- 250	2×10^{18}
400	+ 150	1×10^{18}
	- 100	1×10^{18}
500	+ 350	2×10^{18}
	- 300	2×10^{18}

Of course the requested disposition of running time will be determined by several factors which will only be clear closer to the time.

REFERENCES

- ¹F. J. Hasert, et al., Phys. Lett. 46B, 138 (1973).
- ²Di-Lepton:
- a) A. Benvenuti, et al., Phys. Rev. Lett. 34, 419 (1975).
 - b) B. C. Barish, et al., Phys. Rev. Lett. 36, 939 (1976).
 - c) J. Blietschau, et al., Phys. Lett. 60B, 207 (1976).
 - d) C. Baltay, in Proc. of APS Div. of Particles and Fields, BNL, Upton NY, 6-8 Oct., 1976 (unpublished)
 - e) F. A. Nezrick, et al., Bull. Am. Phys. Soc. 22, 35 (1976).
 - f) J. F. Grivaz, et al., Bull. Am. Phys. Soc. 22, 25 (1976).
 - g) J. von Krogh, et al., Phys. Rev. Lett., 36, 710 (1976).
- Tri-Muon:
- h) A. Benvenuti, et al., Phys. Rev. Lett. 38, 1110 (1977).
 - i) B. C. Barish, et al., Phys. Rev. Lett. 38, 577 (1977).
- ³A. Benvenuti, et al., Phys. Rev. Lett. 36, 1478 (1976).
- ⁴J. von Krogh, Proc. Intl. Conf. on Production of Particles with New Quantum Numbers, Madison, Wisc., 302 (1976).
- ⁵A. Benvenuti, et al., Phys. Rev. Lett. 38, 1110 (1977).
- ⁶D. Cline, private communication.
- ⁷T. Eichten, et al., Phys. Lett. 46B, 281 (1976).
- ⁸F. J. Hasert, et al., Phys. Lett. 46B, 121 (1976).
- ⁹H. Faissner, et al., Proc. Intl. Neutirno Conference, Aachen, 223 (1976).
- ¹⁰L. Mo, et al., Fermilab Proposal 253.
- ¹¹P. C. Soreide, et al., Phys. Rev. Lett. 36, 352 (1976).
and P. G. H. Sandars, "Atomic Physics", 4, ed. G. ZuPutlitz, E. W. Weber, and A. Winnacker (Plenum, NY, 1975).

- ¹²M. L. Perl, et al., Phys. Rev. Lett., 35, 1489 (1975), and SLAC-PUB-1592 and SLAC-PUB-1664.
- ¹³H. Meyer, Proc. of Summer Institute on Part. Phys., SLAC-198, 427 (1976).
- ¹⁴M. Conversi, et al., EP Internal Report (76-20).
- ¹⁵D. Edwards and F. Sciulli, Fermilab TM-660.
- ¹⁶F. Sciulli, Proc. of Calorimeter Workshop, Fermilab, 79 (1975).
- ¹⁷L. M. Sehgal, Phenomenology of Neutrino Reactions, ANL/HEP/PR75-45, (1975).
- ¹⁸A. Bodek, Ph.D. Thesis, MIT (1972), (LNS-COO-3069-116).
- ¹⁹R. J. Stefanski and H. B. White, Neutrino Flux Distributions, FN-292 (1976).
- ²⁰G. 't Hooft, Nucl. Phys. B35, 167 (1971).
- ²¹C. H. Llewellyn Smith, Physics Reports 3C, 261 (1972).
- ²²J. S. Bell and C. H. Llewellyn Smith, Nucl. Phys. B28, 317 (1971).
- ²³S. J. Barish, et al., Phys. Rev. Lett. 33, 448 (1974).
- ²⁴Aachen-CERN-Frascati-Hamburg-Moscow (ITEP) -Napoli-Roma Collaboration, CERN/SPSC/75-59/P49 (Oct. 27, 1975).
- ²⁵B. Ghidini, et al., Nucl. Instr. and Meth., 125, 357 (1975).
- ²⁶S. Mori, et al., Fermilab TM-725.

FIGURE CAPTIONS

- Figure 1: Transverse momentum balance in tri-muon events (from Ref. 6).
- Figure 2: Proposed layout of a low energy neutrino beam for studying neutrino oscillations.
- Figure 3: New neutrino target detector in front of existing Lab C muon spectrometer.
- Figure 4: Sub-module of new detector consisting of plastic flash chambers alternated with 1 cm fiber reinforced cement and 0.6 cm aluminum.
- Figure 5: Full module of new detector consisting of three sub-modules (Fig. 4) plus 0.6 cm Pb and 4.4 cm liquid scintillator.
- Figure 6: The Lab C muon spectrometer, with the two proportional tube hodoscope detector planes.
- Figure 7: Detail of the proportional tube construction. Also shown is the observed pulse height distribution obtained from a prototype detector using an Fe^{55} source.
- Figure 8: Design of the proposed scintillation counters showing their construction and assembly.
- Figure 9: Spatial reconstruction accuracy as a function of the length of the scintillator (from Ref. 25).
- Figure 10: Expected electron energy distributions from
a) neutrino-electron elastic scattering using the two-horn beam, b) di-lepton production, assuming $\mu_{\text{slow}} = e$ (from Ref. 6) and c) deep inelastic ν_e

scattering, using the ν_e beam (Ref. 26).

Figure 11: Several of the prototype 12' x 5' chambers.

Figure 12: Kinematics for the Fermilab narrow band neutrino beam (see Ref. 15). For given neutrino energies, the hadron energy, E_H , is plotted vs. the angle of the hadron shower, θ_H .

Figure 13: Neutrino energy and $y_{\min} = E_{\nu\pi}/E_{\nu K}$ are plotted vs. the radial distance from the center of the neutrino beam for incident neutrinos and antineutrinos.

Figure 14: p_{\perp} distributions of the outgoing electron for $\nu_{\mu e}$ elastic scattering and neutron inverse beta decay (with and without Pauli suppression). The number of events is for 6×10^{18} 400 GeV protons on target, the two-horn neutrino beam and a 360 ton fiducial volume in this detector.

Figure 15: Energy distributions of the outgoing electrons in $\nu_{\mu} e^{-}$ elastic scattering and neutron inverse beta-decay.

Figure 16: p_{\perp} distributions as in Fig. 14, but with experimental \perp resolutions included.

Figure 17: Kinetic energy distribution of the outgoing proton for neutron inverse beta decay (with and without Pauli suppression).

THREE MUON DATA

TRANSVERSE MOMENTUM BALANCE

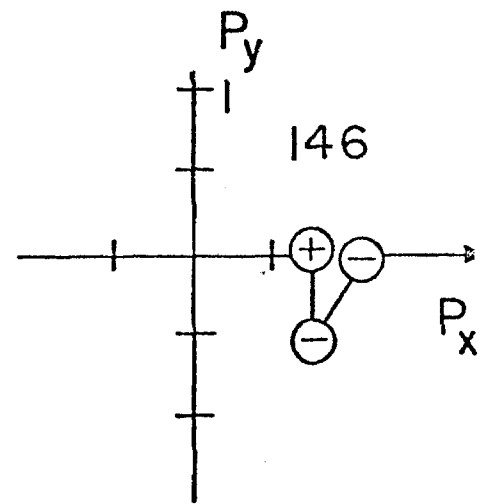
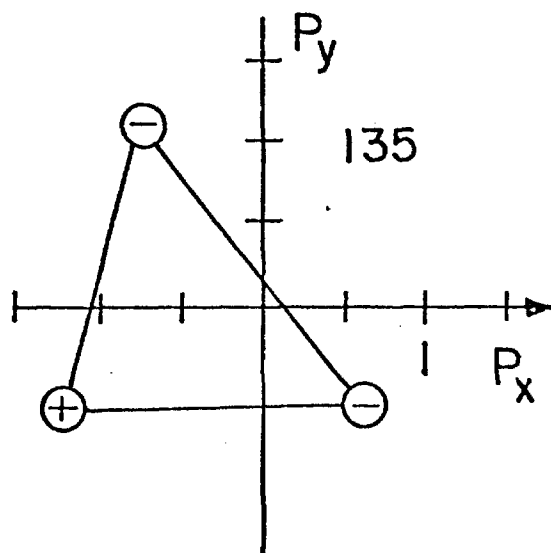
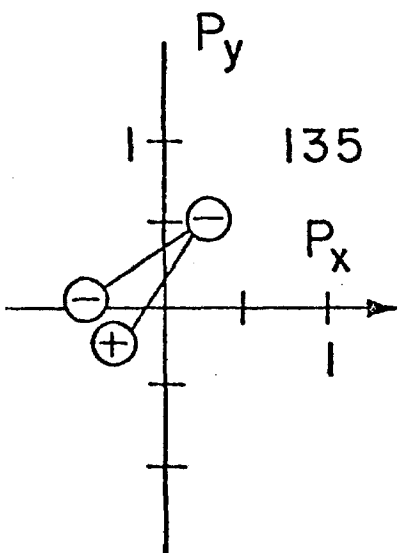
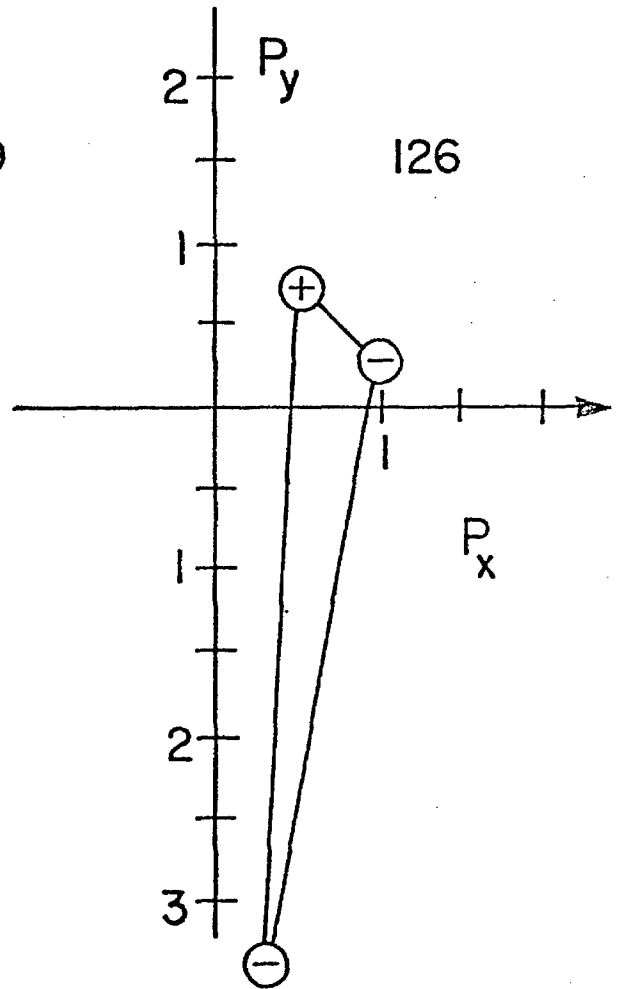
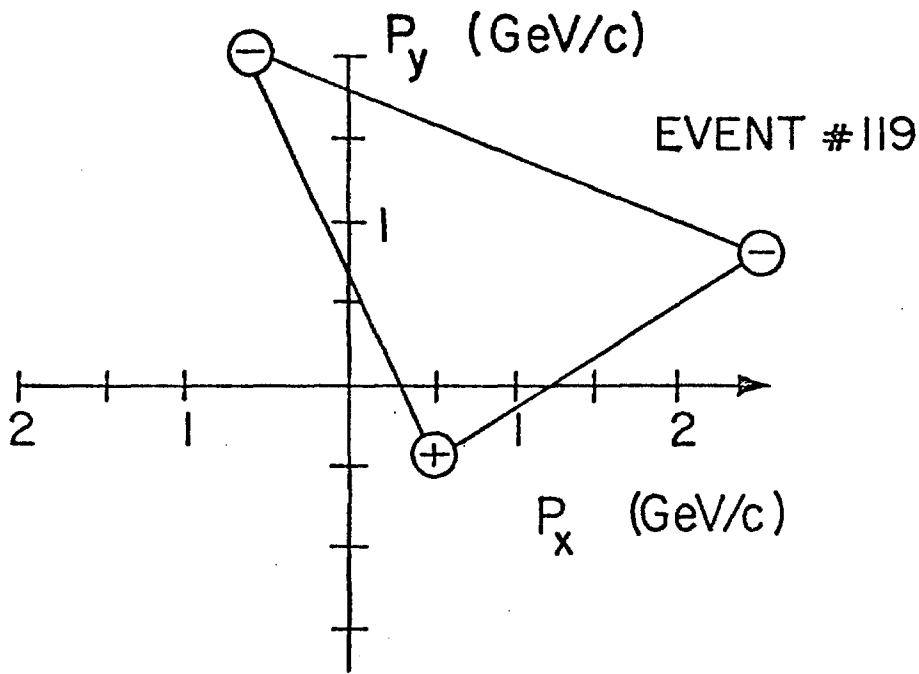
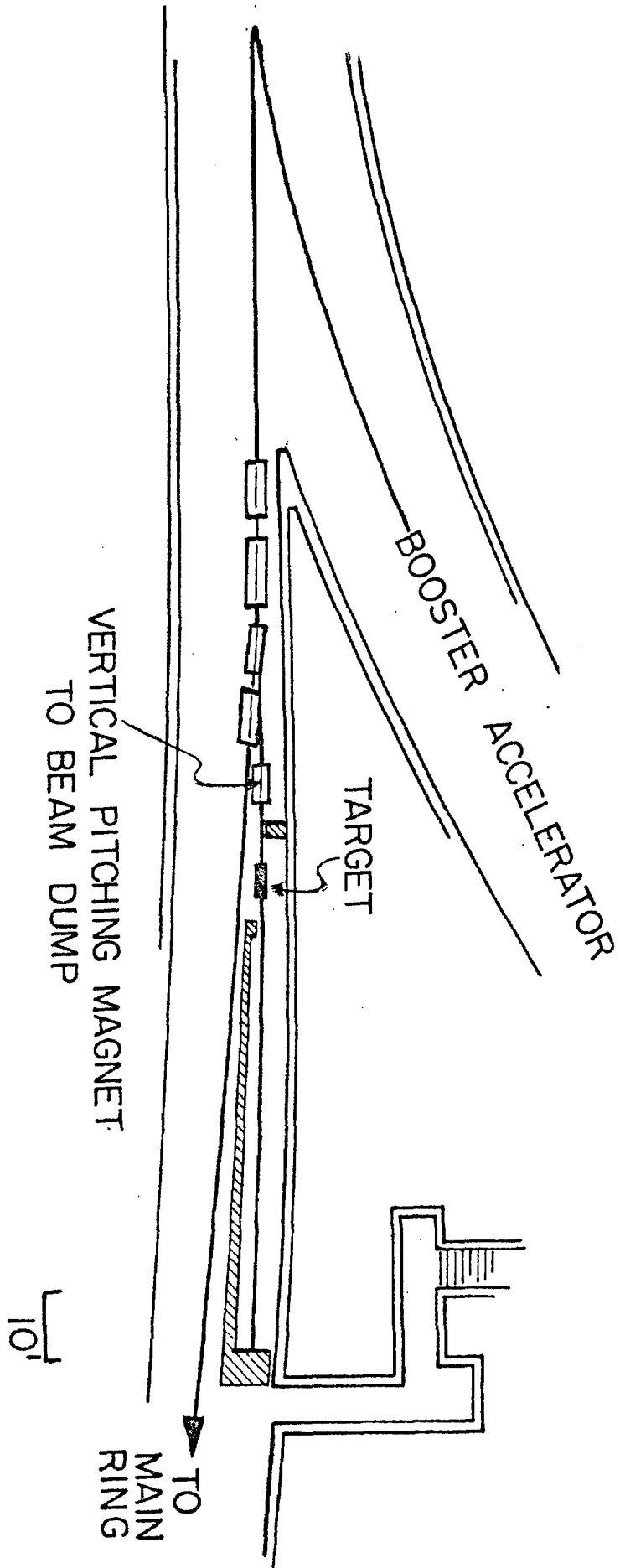


FIG 1



LOW ENERGY NEUTRINO BEAM

Fig. 2

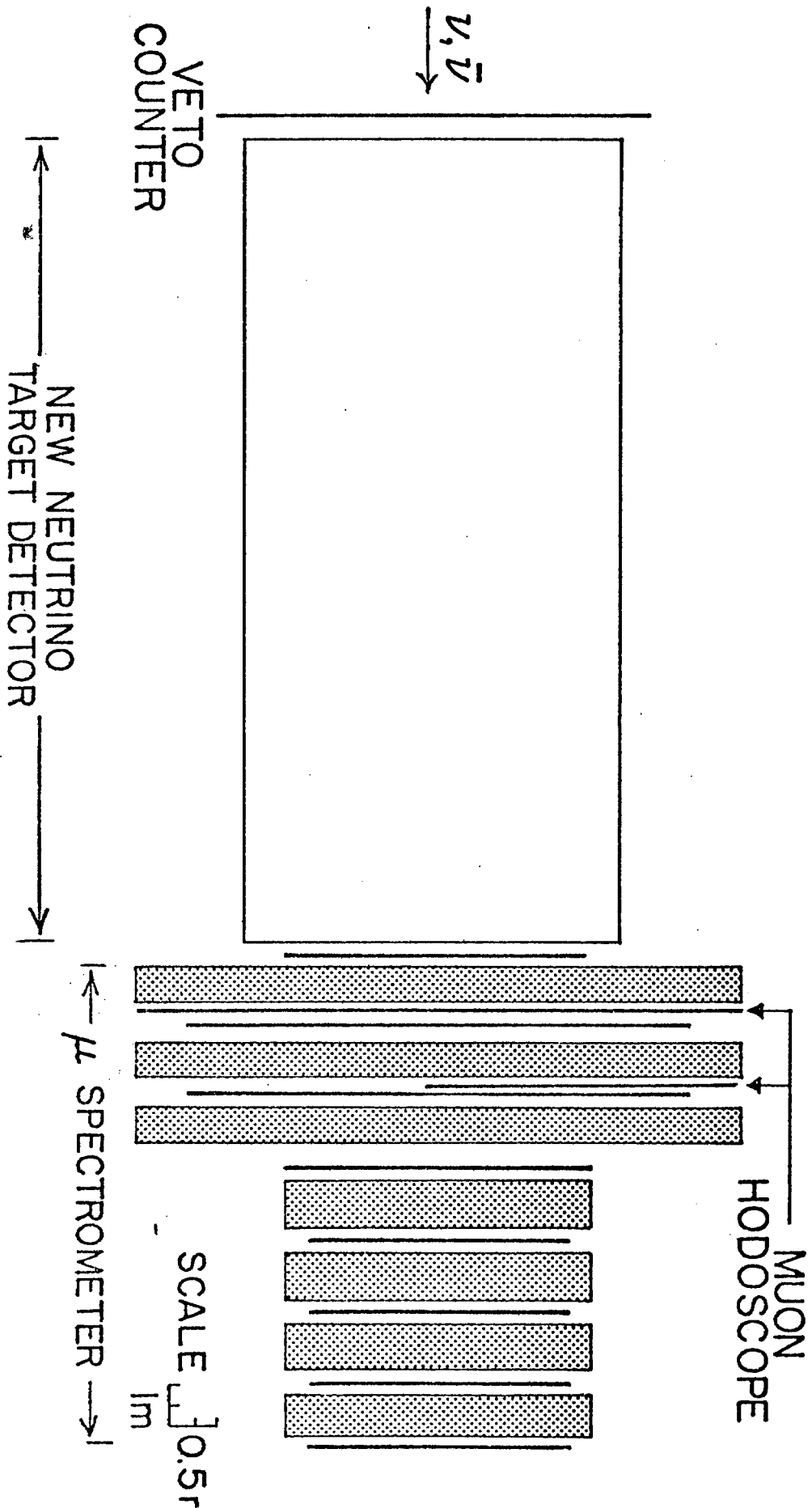
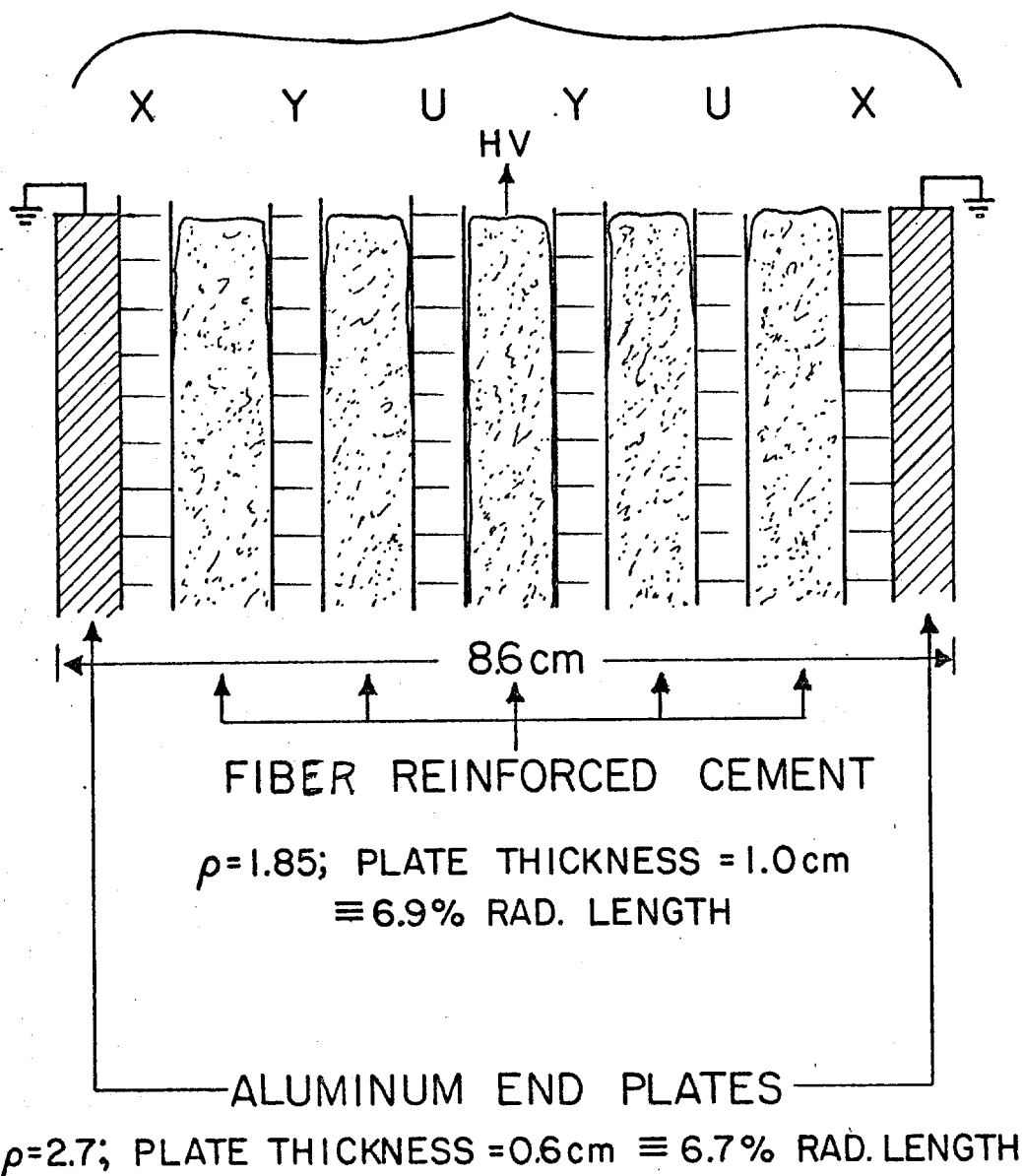


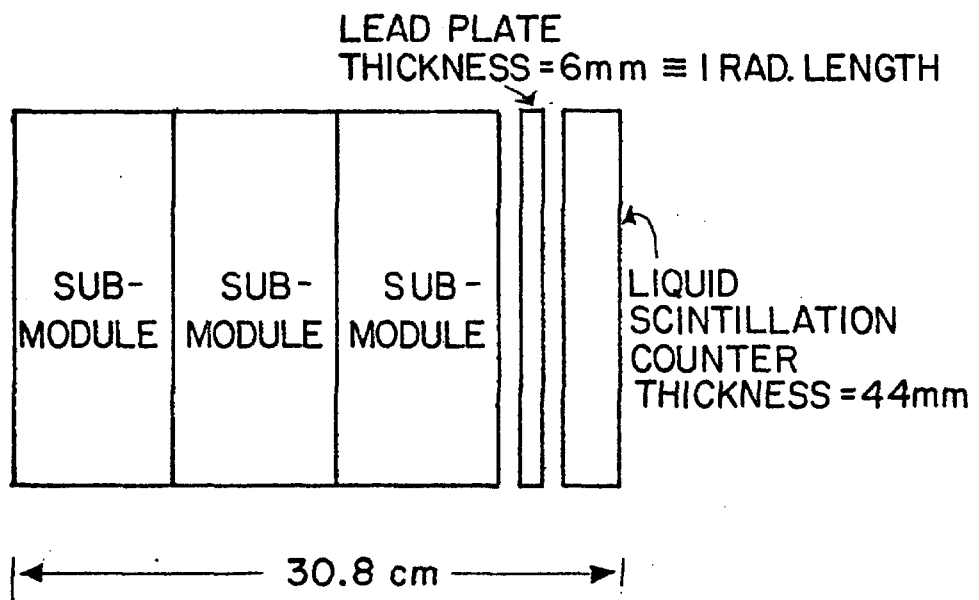
Fig. 3

PLASTIC FLASH CHAMBERS
EACH 0.4cm THICK



ONE SUB-MODULE OF DETECTOR

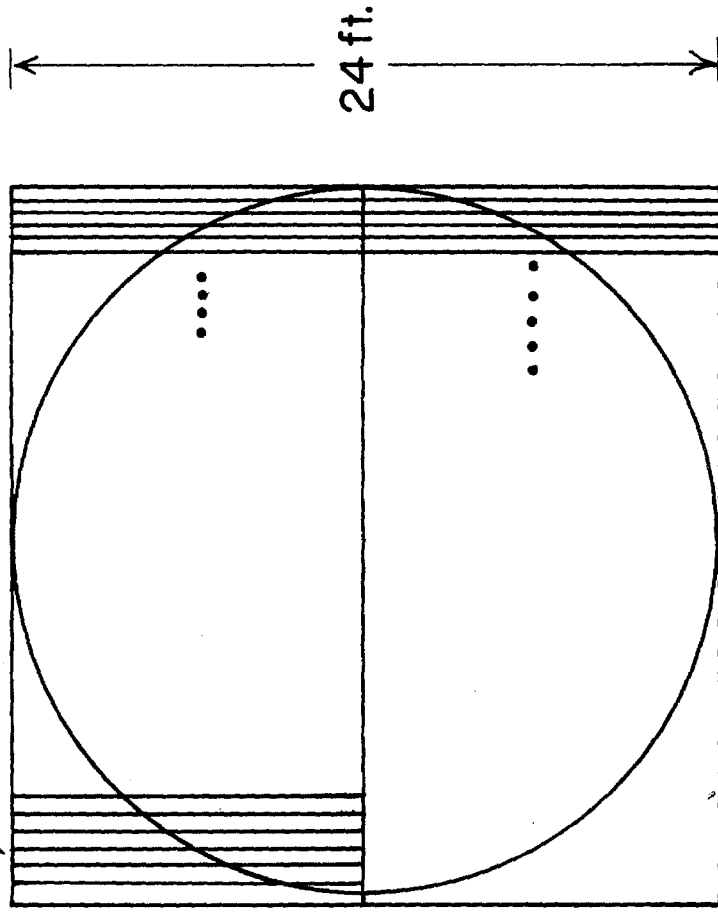
FIG. 4



ONE MODULE OF DETECTOR

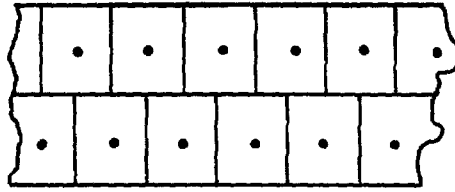
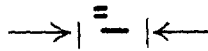
FIG. 5

HODOSCOPE ELEMENTS ($\pm \frac{1}{2}$)



Resolution

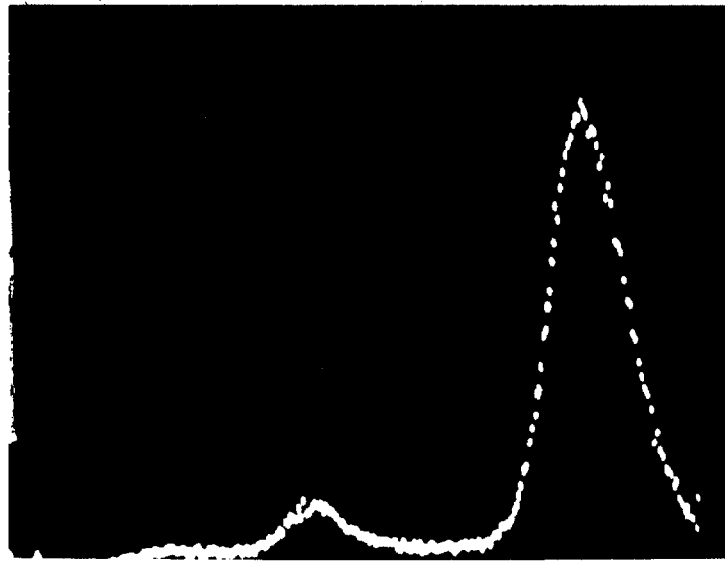
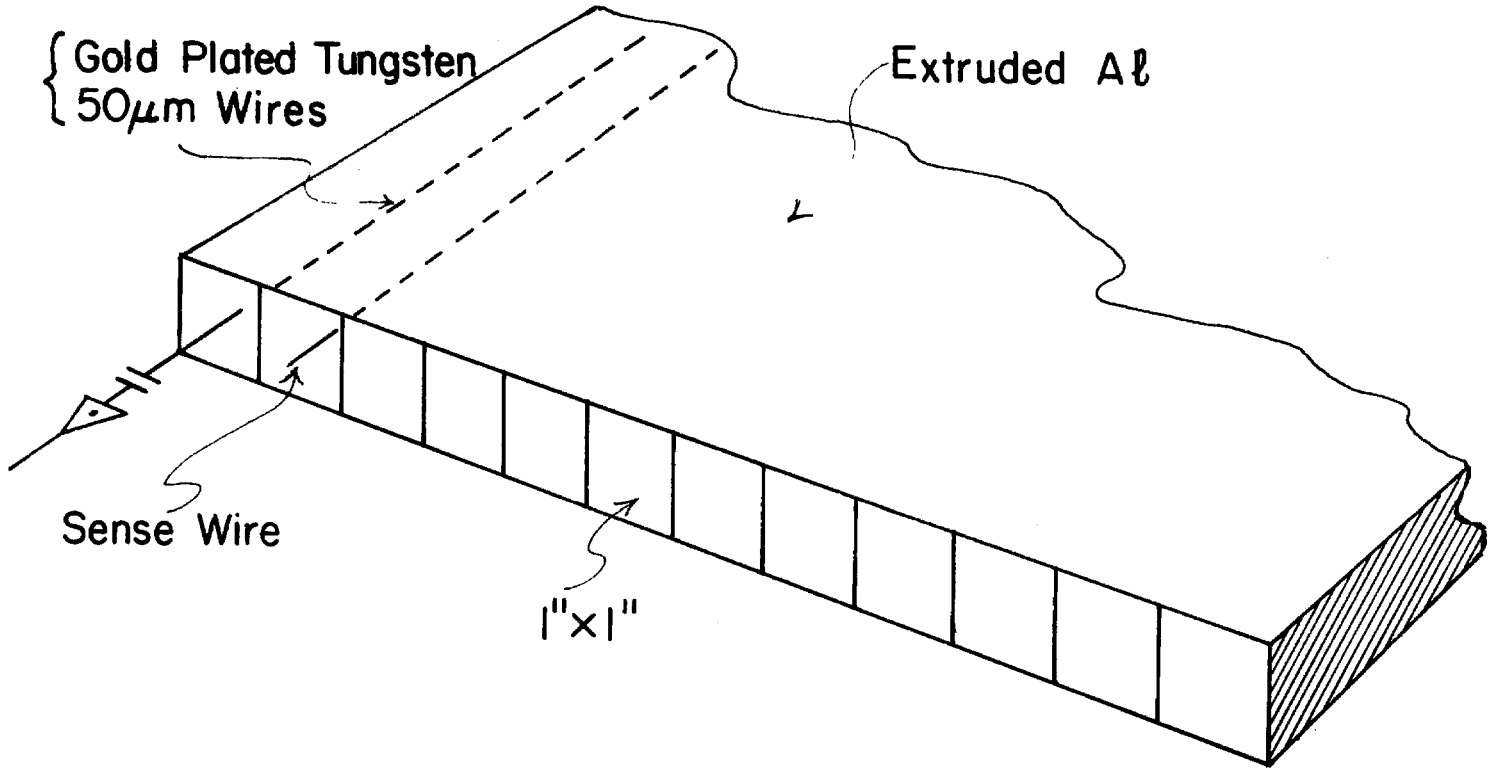
$\sim \pm \frac{1}{4}$



576 Wires / Plane - 2 Planes Total = 1152

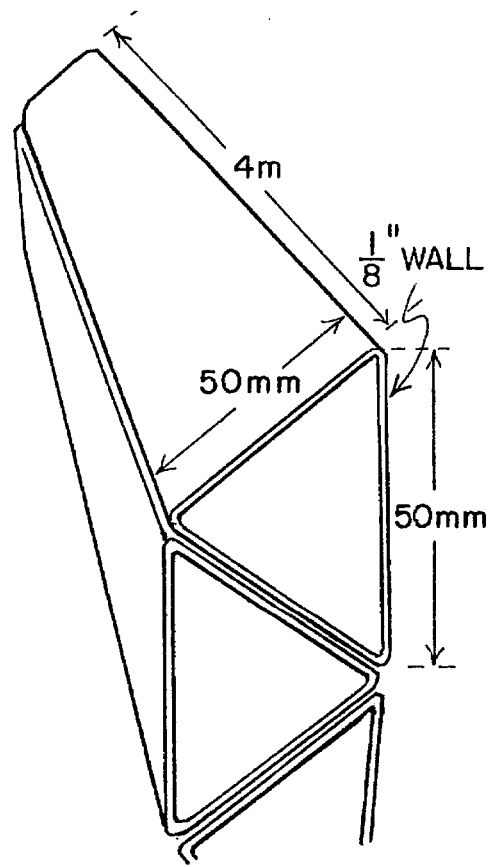
563-67

CONSTRUCTION OF PROPORTIONAL TUBES



OBSERVED PULSE HT DISTRIBUTION
USING F_e 55 SOURCE

figure 7



EXTRUDED TRIANGULAR PLEXIGLASS TUBE COUNTERS
FILLED WITH LIQUID SCINTILLATOR

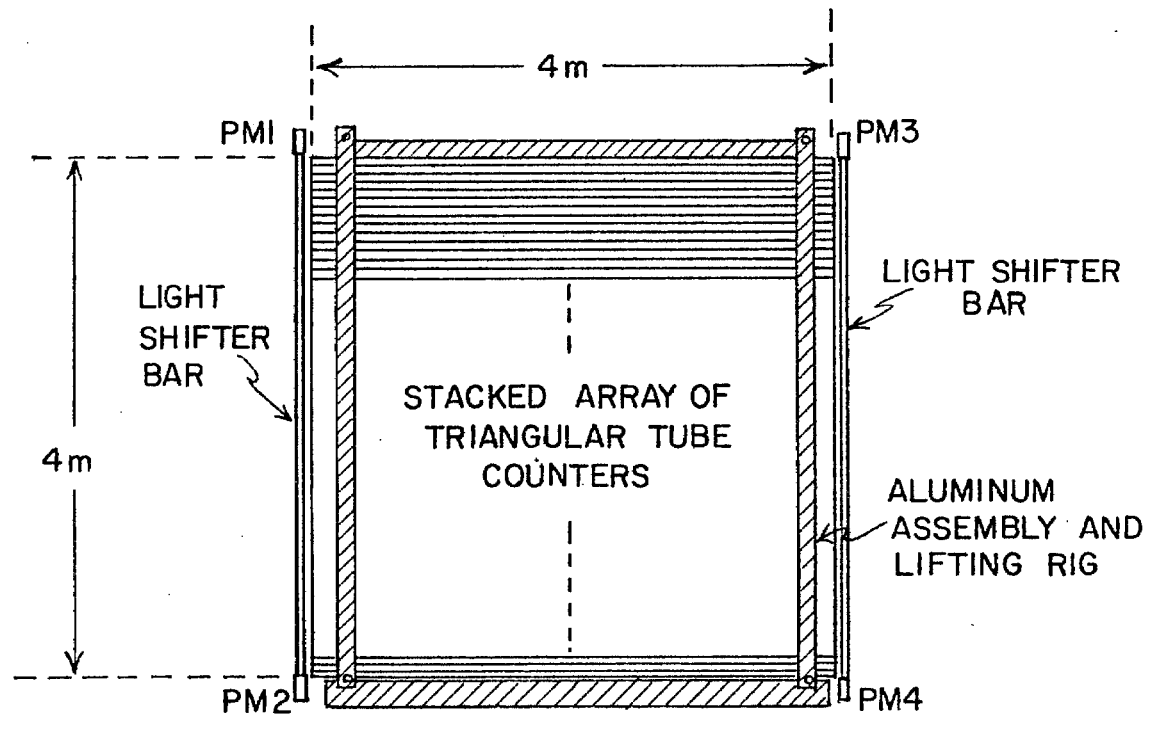


FIG. 8

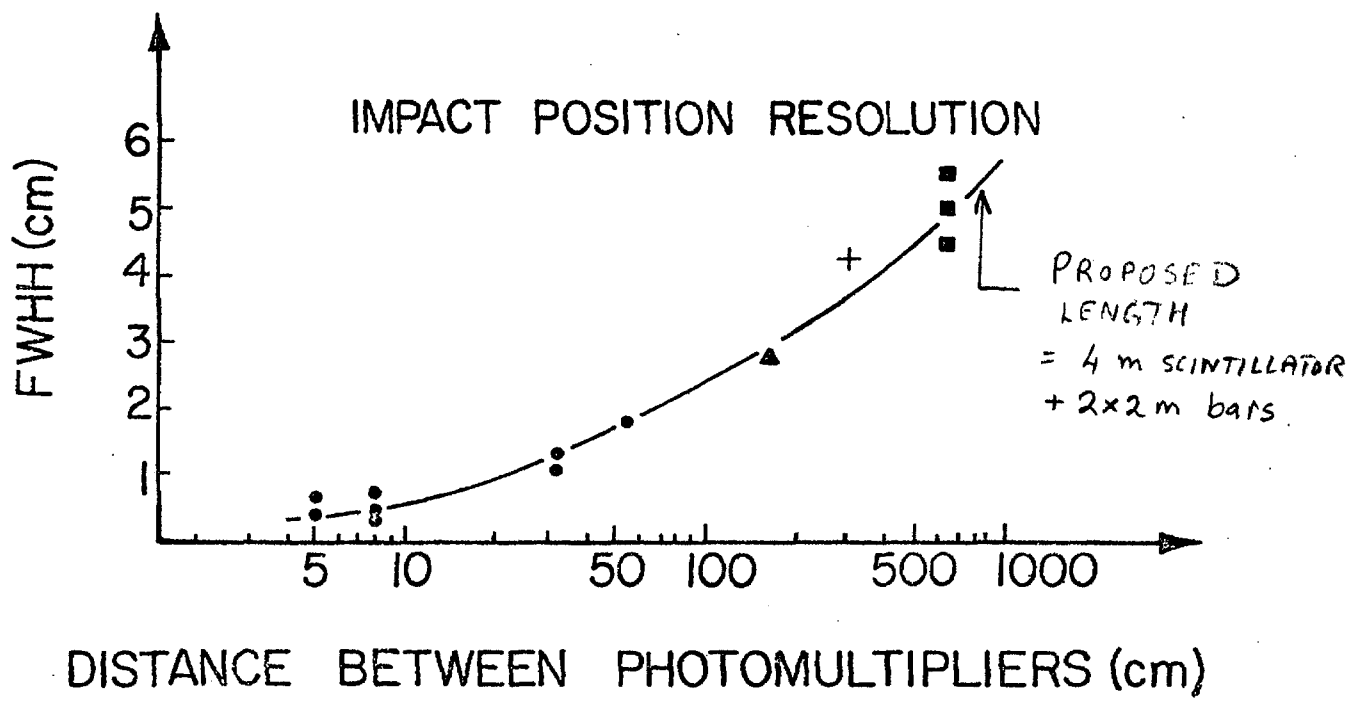
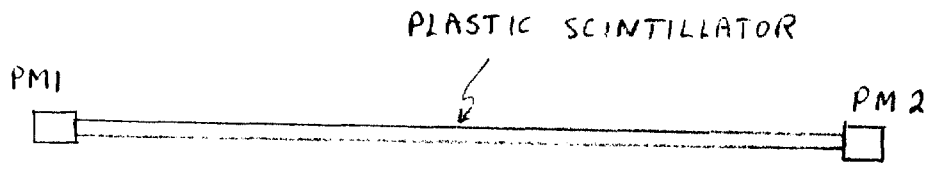


Fig. 9

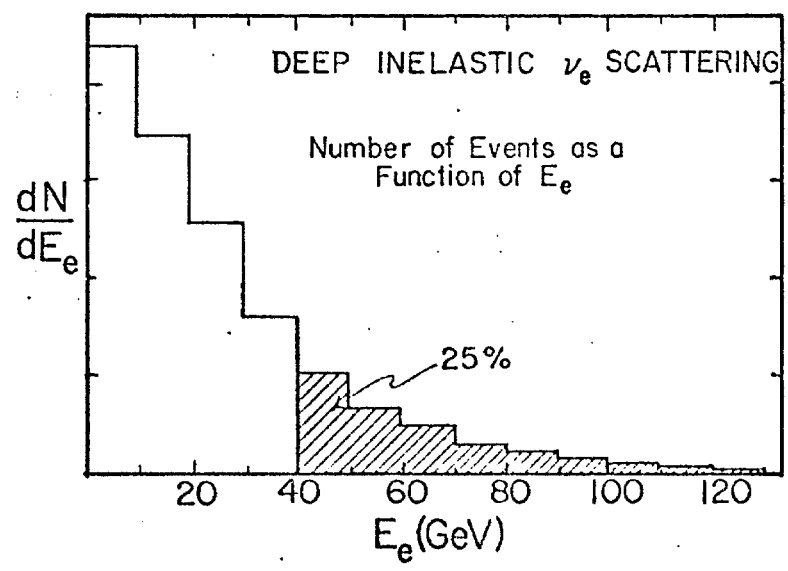
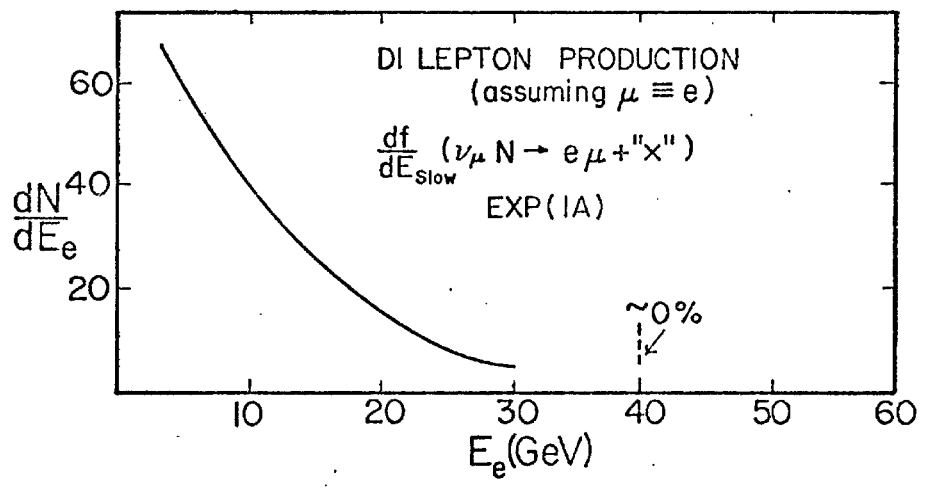
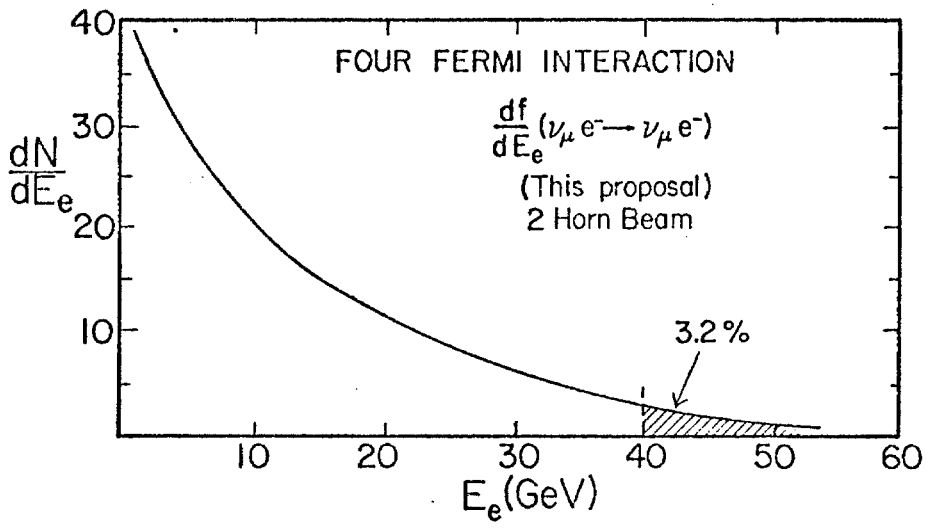


Fig 10

563-71

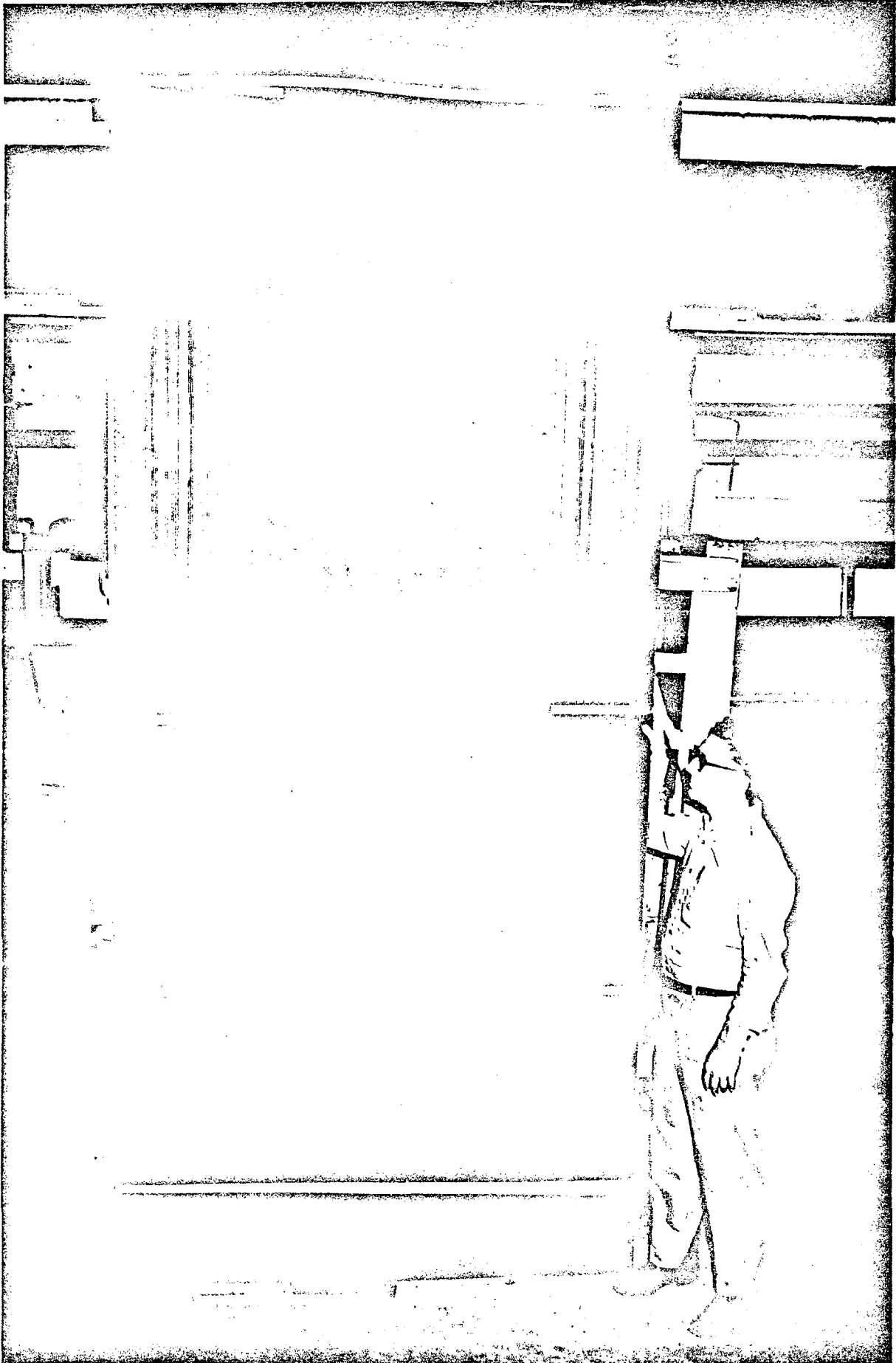


Fig. 11

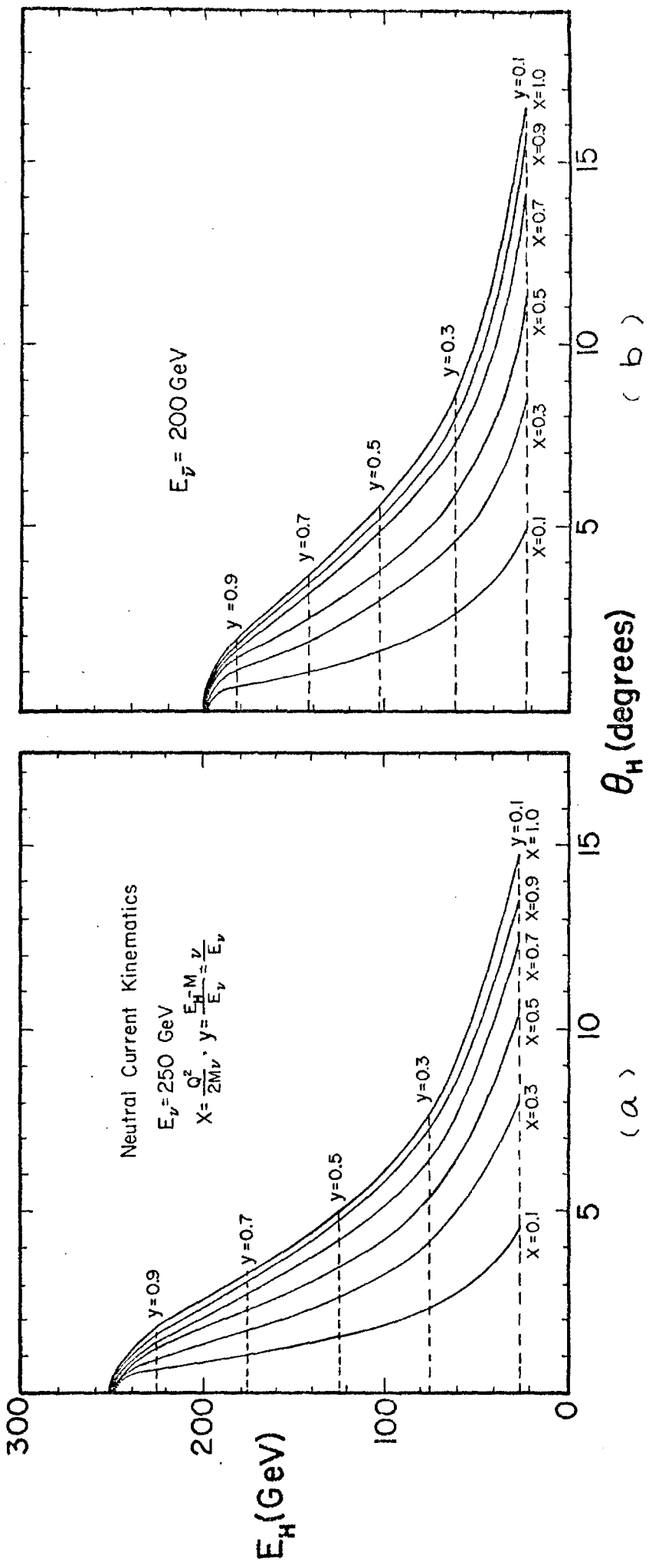


FIG 12.

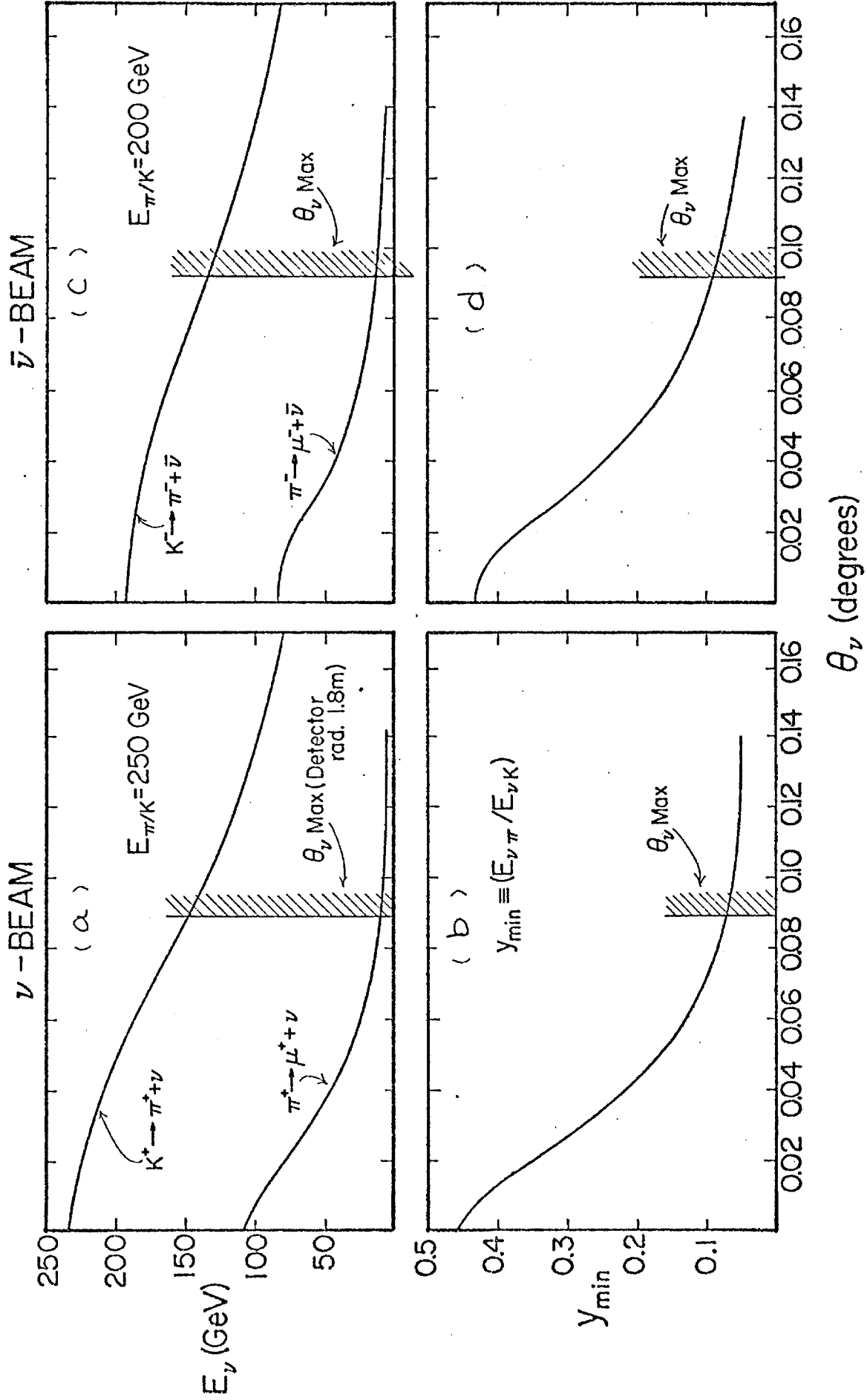


Fig. 13

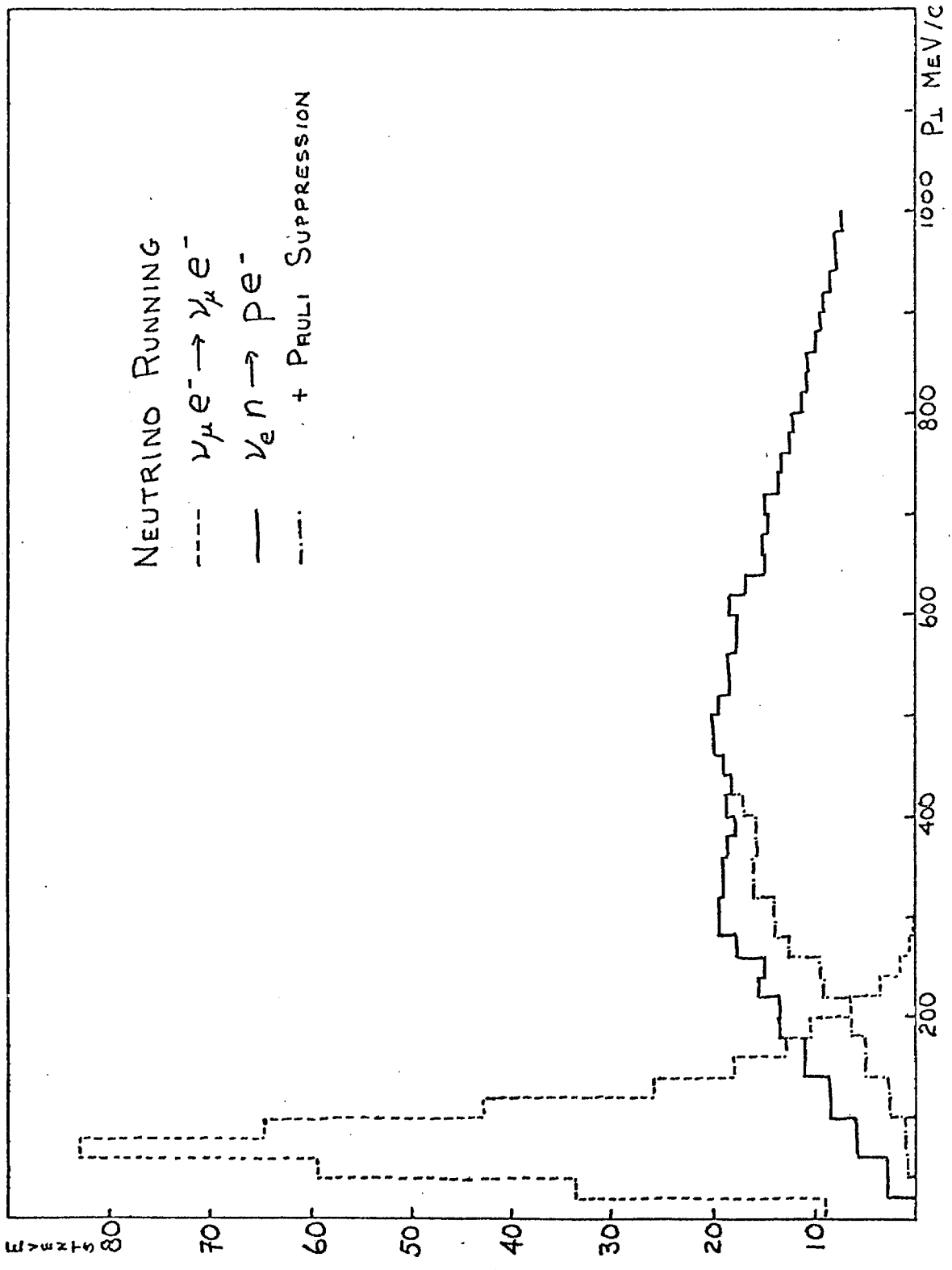


FIG 14

563-75

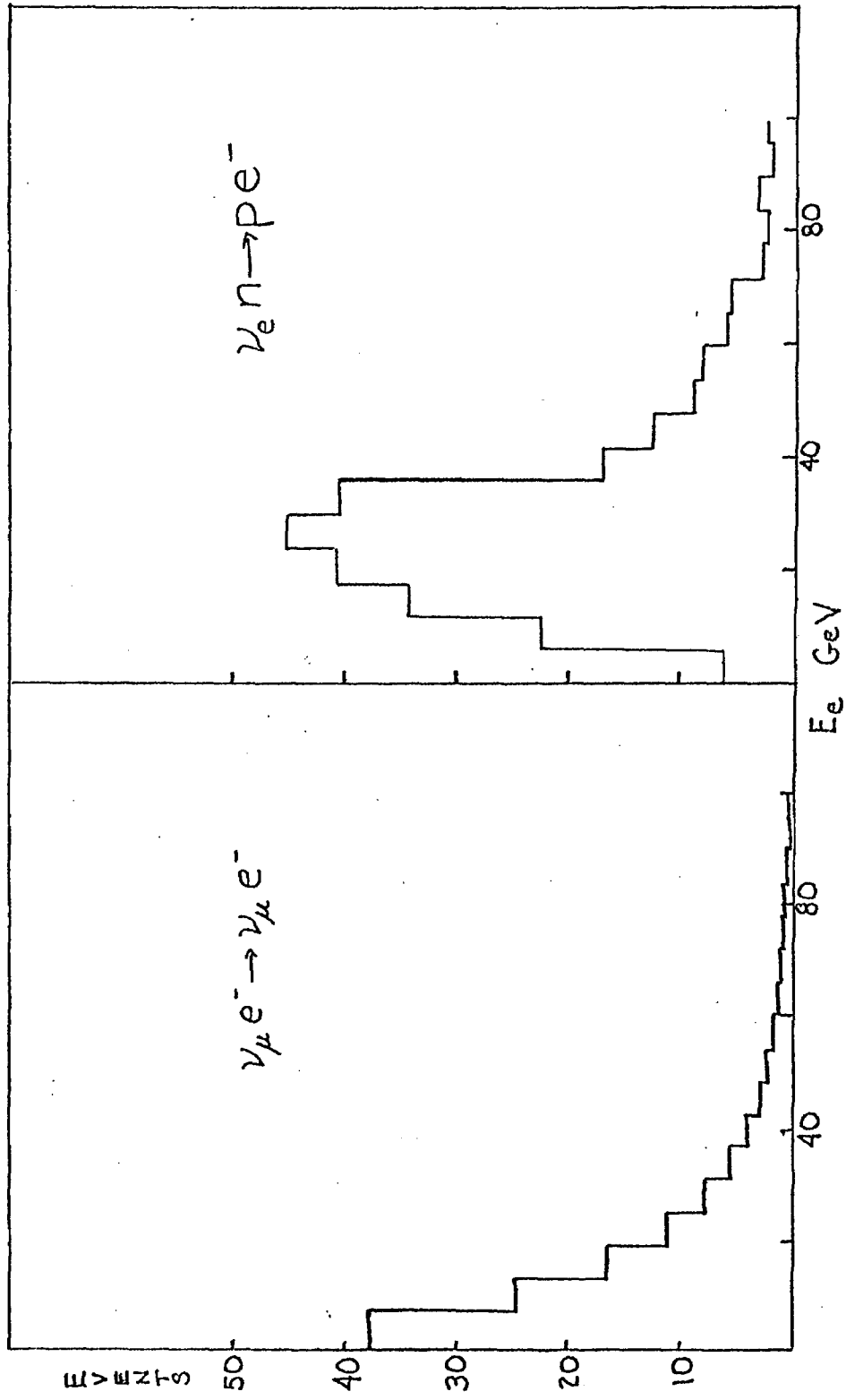


FIG 15

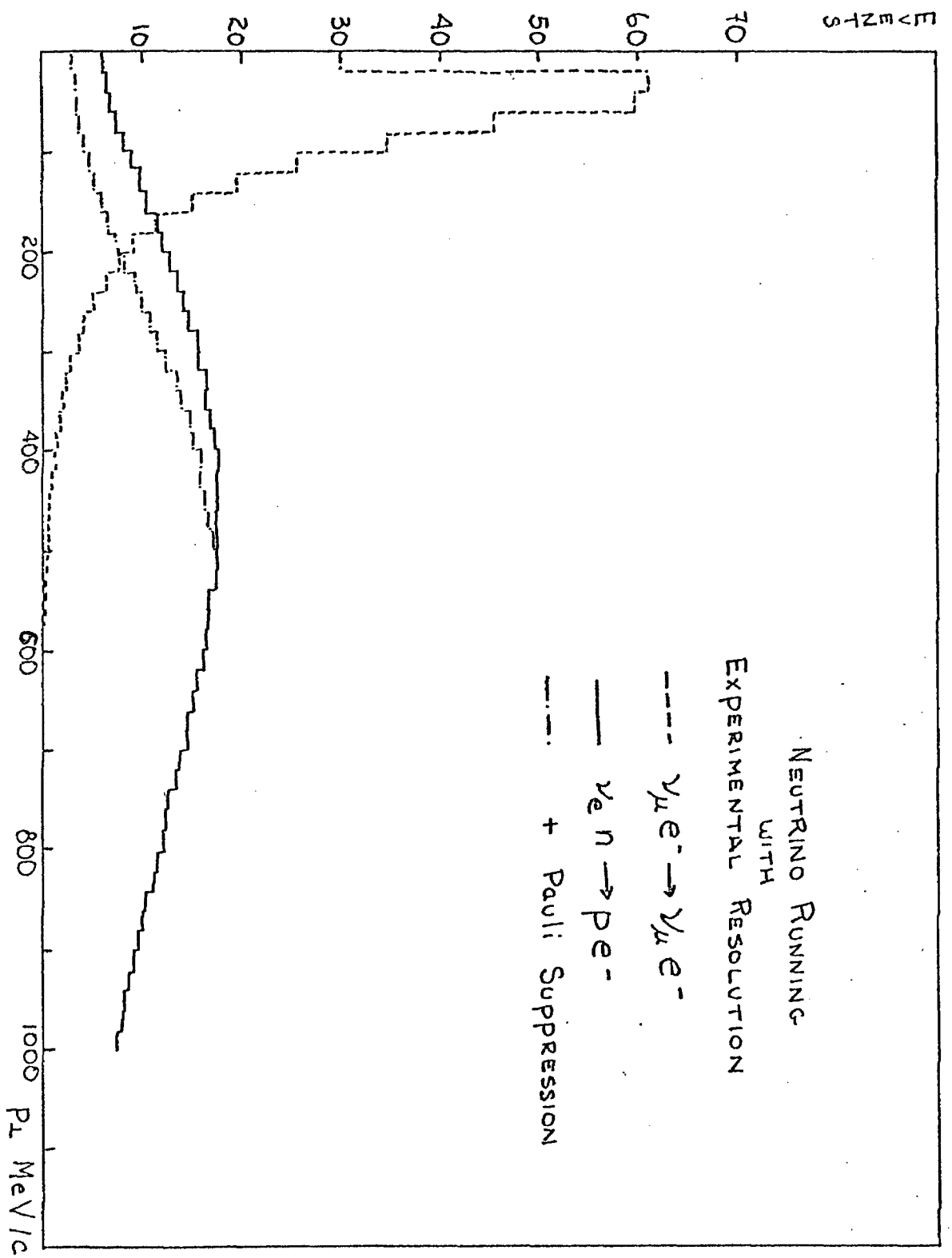


FIG 16

563-77

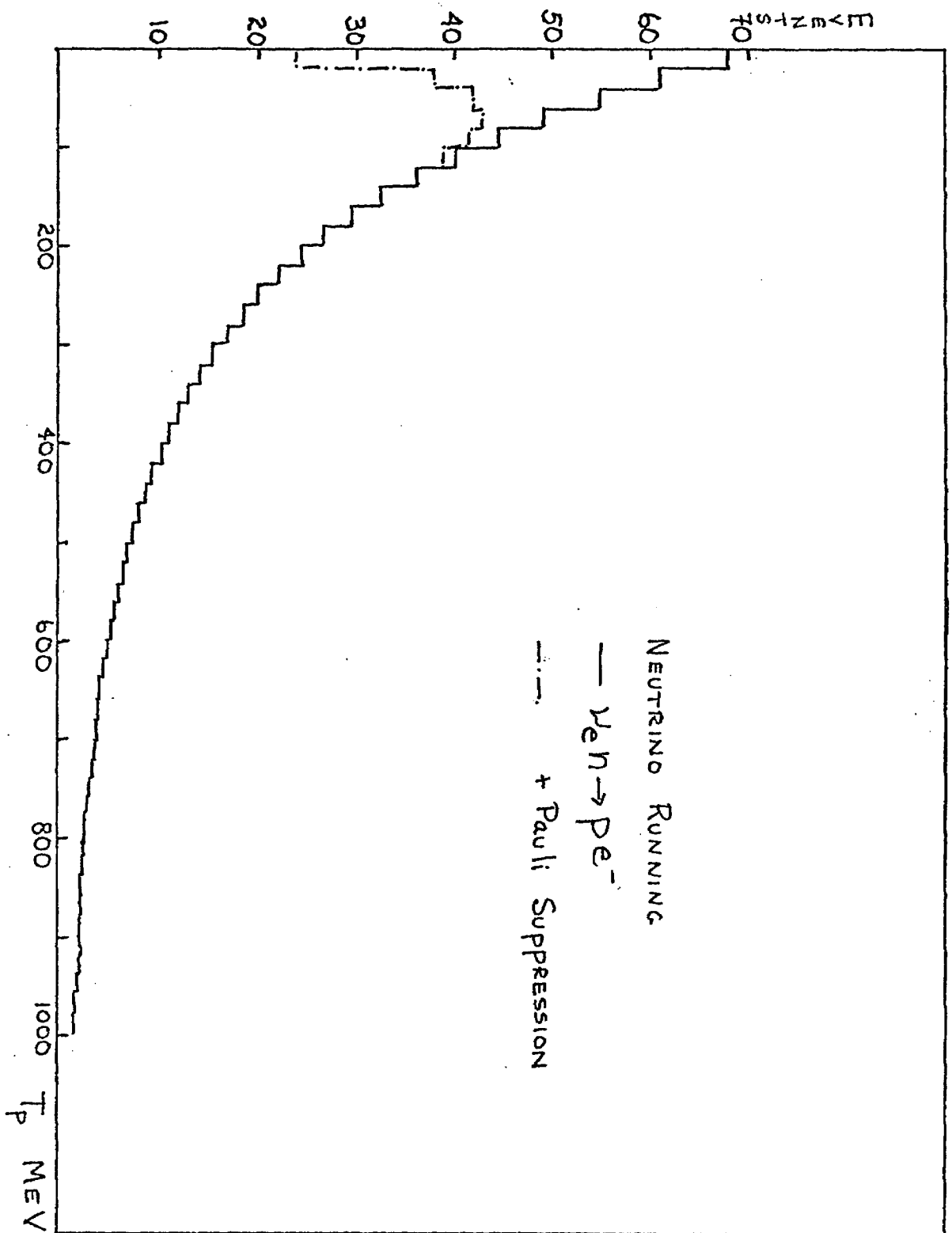


FIG. 17

APPENDIX A
DETECTOR TESTS

A test calorimeter of roughly 1/10 the linear scale of the proposed neutrino detector was constructed and tested in the Meson Lab M5 test beam at Fermilab. The photograph shows the calorimeter. The test beam furnished positive particles in the energy range of 50 to 40 GeV. The beam was composed of roughly 80% π^+ , 20% p and < 3% e^+ . An 18 m long gas Cerenkov counter provided a clean trigger on positrons.

Construction

The test array consisted of 126 polypropylene planes 45 cm x 45 cm wide and 4 mm thick. Every other polypropylene plane was fitted with a gas manifold to make a total of 63 flash chamber planes. A 5 mm plate of lead and a 6.4 mm thick scintillation counter were located every 20 cm in the calorimeter. The total array had 16 radiation lengths and 3.5 collision lengths. The showers were sampled on the average every 24% of a radiation length and every 6% of a collision length. The average density of the calorimeter was 1.7 g/cm^3 . The chamber array was photographed using SO143 film. The layout of the test calorimeter is shown in Fig. Ala.

The flash chambers were made from black polypropylene sheets available at a cost of \$1.5/square meter. The polypropylene sheets were made by an extrusion process with a cell size of 4 mm x 5 mm. The cells were filled with standard Ne (90%) -He (10%) spark chamber gas mixture. Transparent gas manifolds were made from thermo-vacuum formed plastic and glued to the ends

of the polypropylene sheets to form a gas tight chamber (Fig. A 1b). A triggered HV pulse of approximately 8 kV, 100 nsec duration was applied across the 4 mm thick chambers thereby causing a glow discharge in the Ne + He gas which propagates and fills the entire cell where the ionizing particle traversed the chamber. This glow discharge was easily photographed using an 80 mm-f2.8 lens. The flash chamber is capable of detecting many tracks in a given event because each cell is insulated from each other cell, and because there is no DC path for the stored energy of the triggered pulse to ground.

Performance

The response of the test calorimeter to positrons and positive hadrons has been measured in the energy range of 5 to 40 GeV. A set of typical electron showers is shown in Fig. A2a and a typical hadron showers are shown in Fig. A2b. It is apparent from Fig. A2 that the multi-track efficiency is high and that there is little track "robbing". Furthermore the track efficiency appears to be independent of the angle of traversal through the polypropylene cells. In fact we have observed tracks with good efficiency at up to 80 degrees to the normal.

a) Positrons

The number of cells which fire at a given electromagnetic shower depth for various incident energies is shown in Fig. A3. This figure shows the increase of the number of cells with increasing incident energy as well as the slow increase in the depth at the shower maximum. The average total number of cells versus the energy of the incident electron is shown in Fig. A4.

503-80

We find the energy response to be roughly linear up to 20 GeV. For electron energies above 20 GeV the number of electron-positron pairs at the shower maximum is too large to distinguish individual particles with the cell size of 4 mm x 5 mm, and thus the energy response of the calorimeter becomes nonlinear. The energy resolution versus the incident electron energy is shown in Fig. A5. Accounting for the energy response nonlinearity the measured energy resolution is $\Delta E/E < \pm 10\%$ for $5 \leq E_e \leq 40$ GeV. The proposed calorimeter will have a sampling every 14% of X_0 instead of every 24% of X_0 and hence perhaps the energy resolution will improve somewhat as indicated in Fig. A5. We do not require this improvement however.

A preliminary measurement of the angular resolution of the incident electron direction was computed by a least squares fit to the center of gravity of the number of cells firing at different shower depths. A typical fit to an electromagnetic shower is shown in Fig. A6a. The resulting angular resolution (projected angle) for incident electrons for 25 events at incident energies of 10 and 20 GeV (added together) is shown in Fig. A6b where it is seen that $\sigma(\theta_e) = 4.3$ mrad. This resolution will be improved at higher energies since the shower propagates to a greater depth with increasing incident energy.

b) Hadrons

Hadron showers have been measured in the energy range, 5 to 40 GeV. Due to the small number of collision lengths (3.5) in the test array, the hadron shower could not be fully contained. However the most important feature of the hadron response, namely energy flow direction resolution of the calorimeter could be determined.

First, hadron showers are readily distinguishable from electron showers because of the larger average p_{\perp} in a hadron collision and the slower shower development curve of the hadron showers. We have checked this electron/hadron discrimination by taking data with no selection on the incident particle type and attempting to identify electrons in the data. A simple criterion was used to identify hadrons. If an event downstream of two radiation lengths contained at least one track, defined as at least nine cells forming a line without adjacent firing cells, then the incident particle was called a hadron - otherwise it was identified as an electron. These measured electron/hadron (e/h) ratios for various incident energies were compared with the measured e/h ratios determined by the gas Cerenkov counter. The electron/hadron ratios determined by the flash chamber detector and the Cerenkov counter were consistent with each other. We conclude that hadron rejection is at least 100:1 at 30 and 40 GeV.

By using the hadron cascade information through 3 collision lengths we have measured the angular resolution of the hadron energy flow by performing a least squares fit to the vertex of

the first hadron interaction and the center of gravity of the hadron cascade at intervals of 0.06λ up to 3λ . Samples of the hadron cascade data are shown in figures A7a, b and c for various incident energies. In these figures the data are shown for clarity only every ninth detecting plane, i.e., 0.54λ . The angular resolution of the shower is shown plotted in Fig. A-8 for the case of 20 GeV incident hadrons. The projected angle resolution is measured to be $\sigma(\theta_H) = 24$ mrad. This gives a polar angle error of $\sigma(\theta_H) = 34$ mrad. The energy dependence of $\sigma(\theta_H)$ is shown in Fig. A9 for 20 and 40 GeV. A linear fit to the data is $\sigma(\theta_H) = 8 + 520/E_H$ mrad.

Extensive calculations and measurements on the angular resolution of the hadron energy flow have been made in recent years at CERN.²⁴ A detector was considered which consisted of many strips, extending over the full width of the calorimeter, horizontally and vertically in alternate planes. If the Z-axis is in the direction of the incident neutrino beam, and the interaction vertex is at the origin of the coordinates, then the direction of the hadronic shower, θ_H , is determined by

$$\theta_H = \left(\left\langle \frac{x}{Z} \right\rangle^2 + \left\langle \frac{y}{Z} \right\rangle^2 \right)^{1/2}$$

where the averaging is done over all detector planes and over all detector elements struck by a traversing particle, weighted with the number of traversals. The angular resolution was determined as a function of detector cell width and of sampling step size between detector planes. The results of this Monte Carlo calculation are shown in Fig. A10 for both aluminum and iron plates and

a hadron energy of 100 GeV. The energy dependence of the angular resolution was investigated and in the range 20-200 GeV could be approximated by $\sigma(\theta_H) = 6 \left(\frac{100}{E_H} \right)^{0.8}$ mrad for the case of zero sampling step size and zero detector cell width. This corresponds to the best attainable situation possible. The "theoretical limiting" angular resolution $\sigma(\theta_H) = 6 \left(\frac{100}{E_H} \right)^{0.8}$ mrad is plotted as the dashed curve in Fig. A9. The data is about 30% higher than the dashed curve indicating that the detector provides a resolution which is close to the theoretical limit for defining the direction of hadron energy flow. It is clear from figures A7a, b and c that some of the hadron cascade energy is leaking out the sides and back of the calorimeter. In the neutral current reactions in the neutrino detector we have defined a fiducial tonnage (300 tons out of a total 500 tons) such that there will be negligible energy loss. We therefore expect an improvement in energy flow angular resolution with the proposed neutrino detector. In addition, an energy dependence of the resolution of the form $E_H^{-0.8}$, as suggested theoretically, would tend to improve the resolution at large hadron energies compared to that extrapolated by our linear fit $\sigma(\theta_H) = 8 + \frac{520}{E_H}$ mrad. For the purpose of making a conservative, experimentally based estimate of resolution in the neutral current scaling variables x and y, we have used our linear fit to $\sigma(\theta)_H$ in the Monte Carlo simulation described in the text. We therefore regard the resolutions in x and y as lower limits to that which we will achieve ultimately.

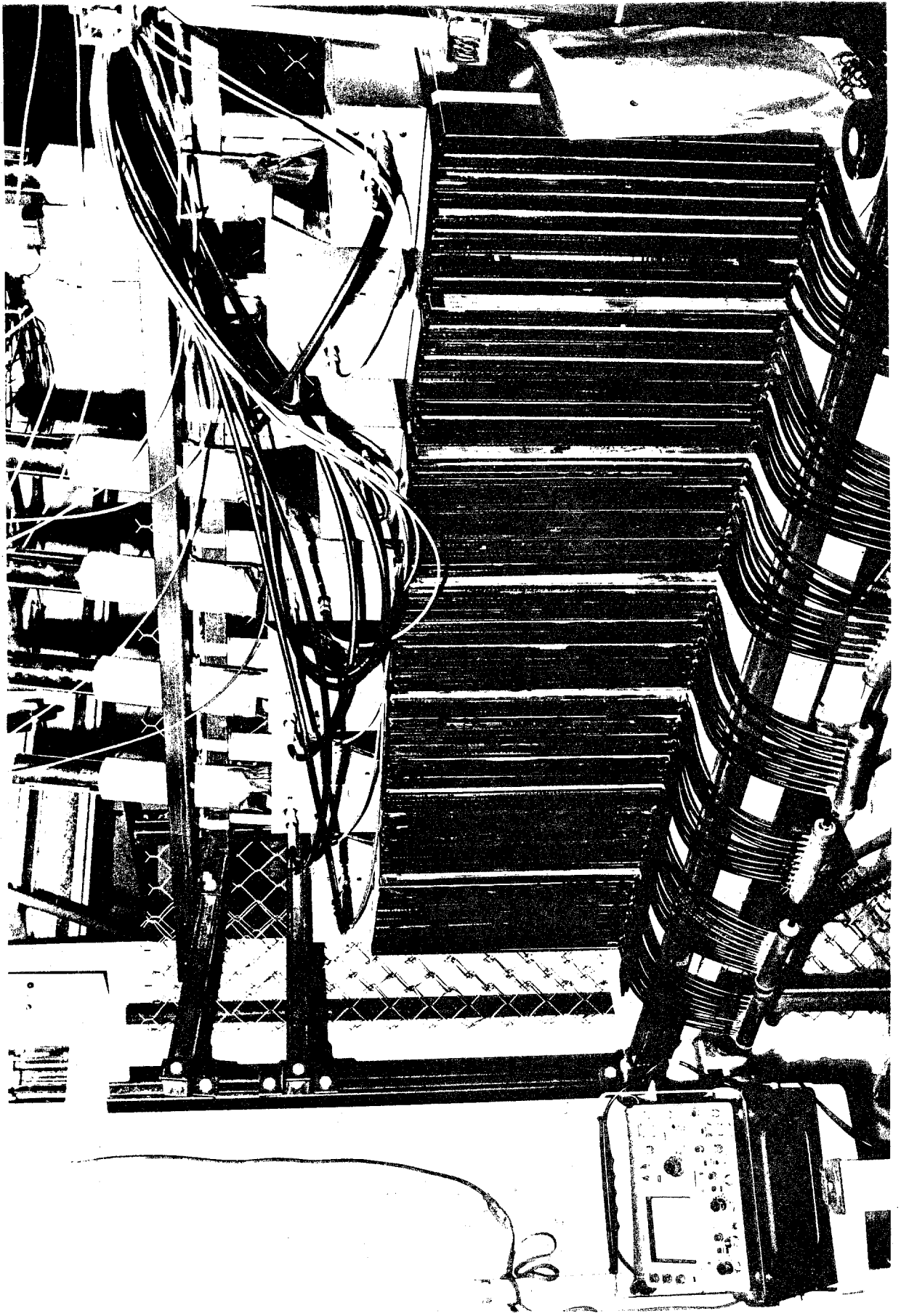
APPENDIX A

FIGURE CAPTIONS

- Photograph: Pictured is the test apparatus used in the M5 beam. The tubes at the bottom of photograph are for the gas input. The boxes on the top are 7 spark gaps, each of which is used to pulse 9 flash chambers. Visible are the six scintillation counters placed behind the 5 mm lead sheets. The chambers are viewed from the left.
- Fig. A-1a: Layout of the test apparatus showing placement of lead, scintillation counters and arrangement of the polypropylene sheets.
- Fig. A-1b: Details of one flash chamber gap showing the 6.4 mm aluminum electrodes, the polypropylene sheet and the gas manifold.
- Fig. A-2a: Sample positron showers at 5 GeV to 40 GeV. These events were obtained by requiring the gas Cerenkov counter set for electrons only to fire. The number of cells which fire is proportional to the energy.
- Fig. A-2b: Sample hadronic showers. Notice the larger average opening angle than in electromagnetic showers, and the large ionization fluctuations due to converting γ rays from π^0 decay.

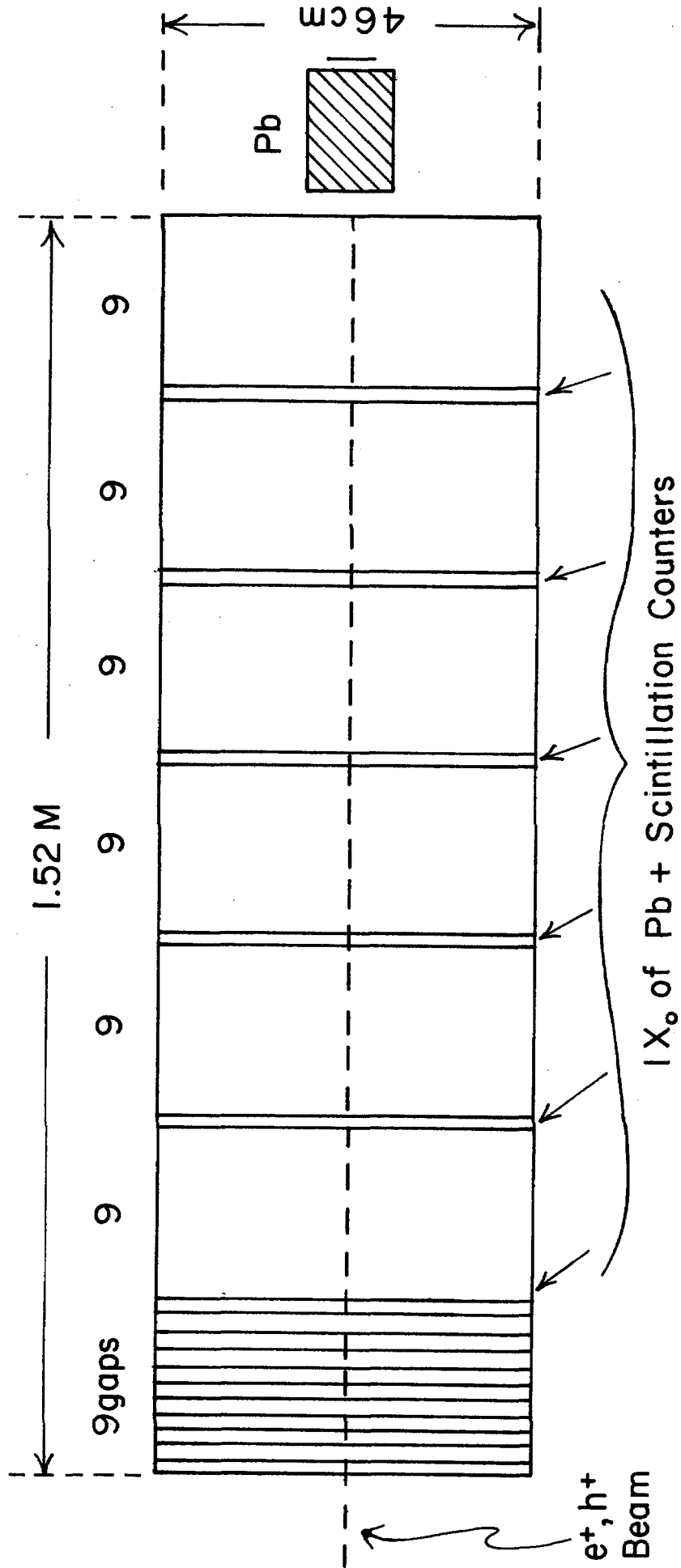
- Fig. A-3: Electromagnetic shower transition curve, showing the number of tubes (cells) which fire as a function of depth in the shower for several incident energies.
- Fig. A-4: The total number of tubes which fire in an electromagnetic shower vs. the incident positron energy. The nonlinearity sets in at $E_e \approx 20$ GeV.
- Fig. A-5: Electron energy resolution HWHM in percent. The nonlinear energy response of Fig. A-4 has been folded in with the increased resolution in the tube count with increasing energy.
- Fig. A-6a: The position of the shower center of gravity in arbitrary units vs. the shower depth.
- Fig. A-6b: The measured resolution of the projected angle for electromagnetic showers at $E_e \approx 15$ GeV. These data were obtained from a least squares fit to the shower center of gravity vs. the shower depths.
- Fig. A-7a: The hadron shower transition center at 10 GeV. Plotted are the number of firing cells vs. the lateral position for various shower depths in the detector. (A collision length is 43.4 cm in the test apparatus.)
- Fig. A-7b: Hadron shower development at 20 GeV.
- Fig. A-7c: Hadron shower development at 40 GeV.

- Fig. A-8: The hadron energy flow projected angular resolution at 20 GeV .
- Fig. A-9: The polar angular resolution of the hadron energy flow vs. the reciprocal of the incident hadron energy. The theoretical limit is from Ref. 24.
- Fig. A-10a: The resolution $\sigma(\theta_H)$ of the hadron shown direction as a function of the widths of the detector elements from Ref. 24.
- Fig. A-10b: The resolution $\sigma(\theta_H)$ vs. the sampling setup from Ref. 24.



FLASH CHAMBER TESTS

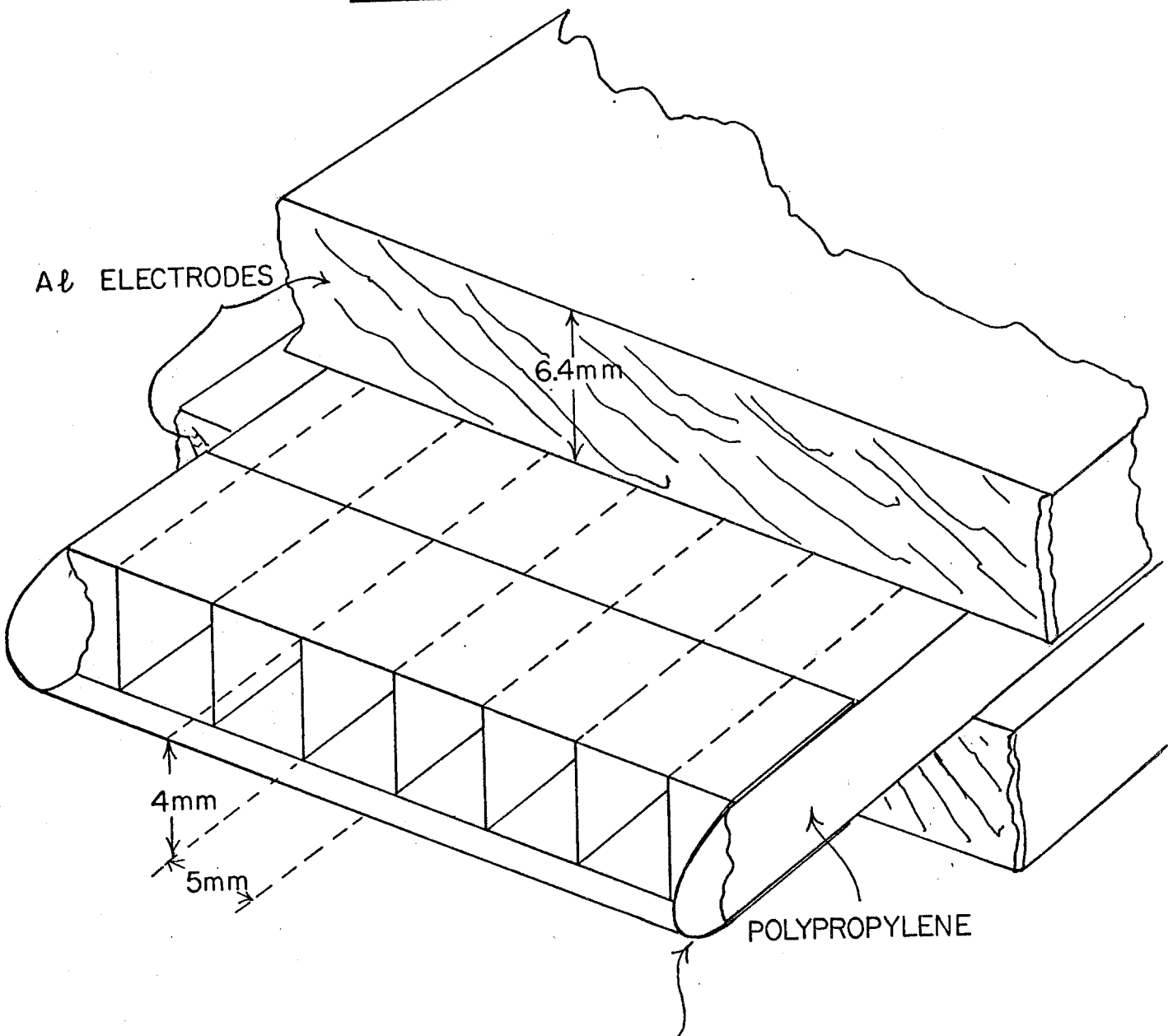
16 X_0 , 3.5 λ_0 , 63 Chambers, X_0 Sampling = 24% of X_0 (14% in Al)
 (6 of Pb + 7 of Al) (One View) λ_0 Sampling = 6 % of λ_0



5 GeV $\leq E \leq$ 40 GeV (Cerenkov Counters to define e^+)

FigA-1a

FLASH CHAMBER GAP



AL ELECTRODES

6.4mm

4mm

5mm

POLYPROPYLENE

GAS MANIFOLD

Fig 1 b

563-90

POSITRONS

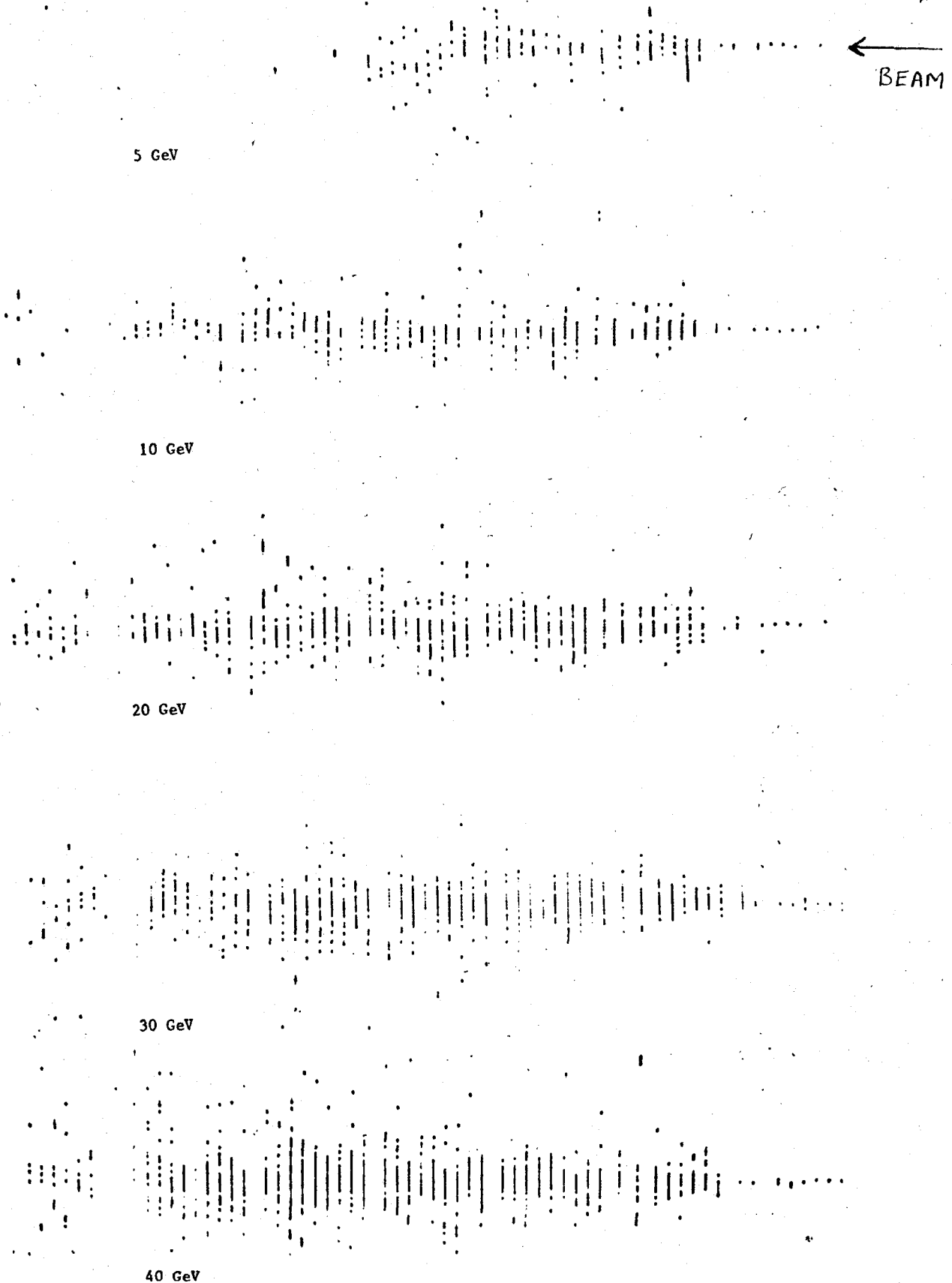


FIG. A-2a.

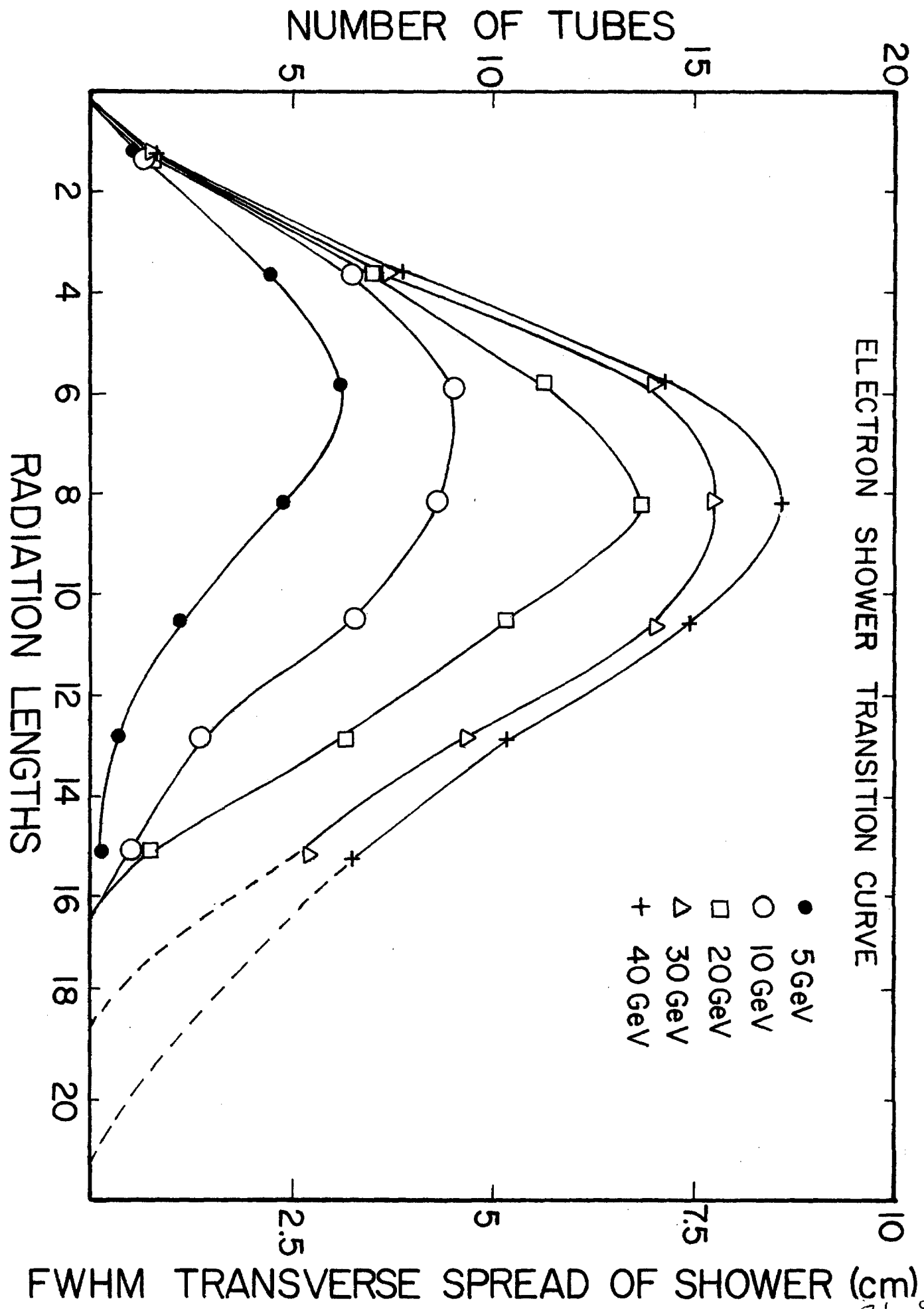


Fig. A-3

FIG. A-26

30 GeV



20 GeV



20 GeV



HADRONS

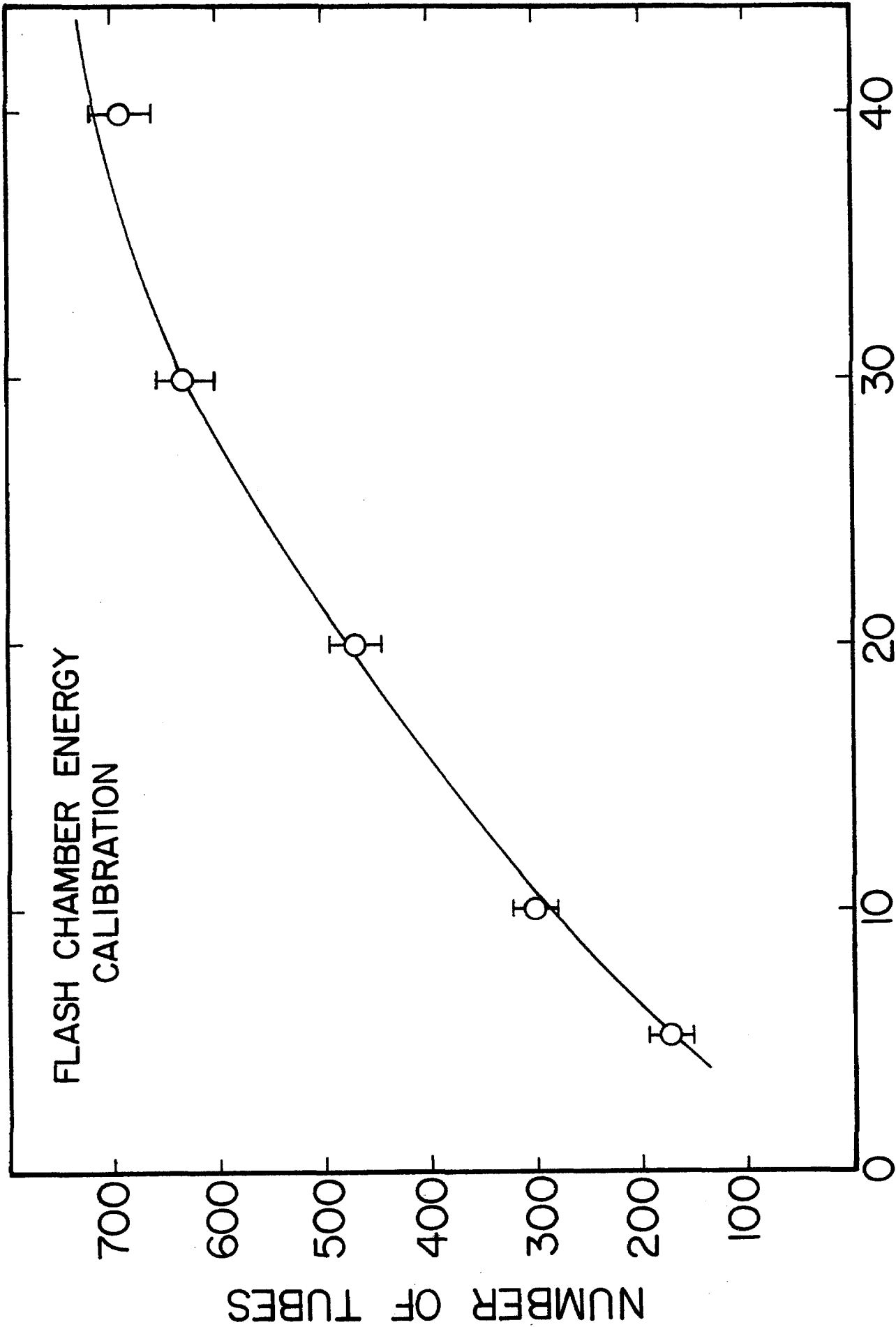


Fig A-4

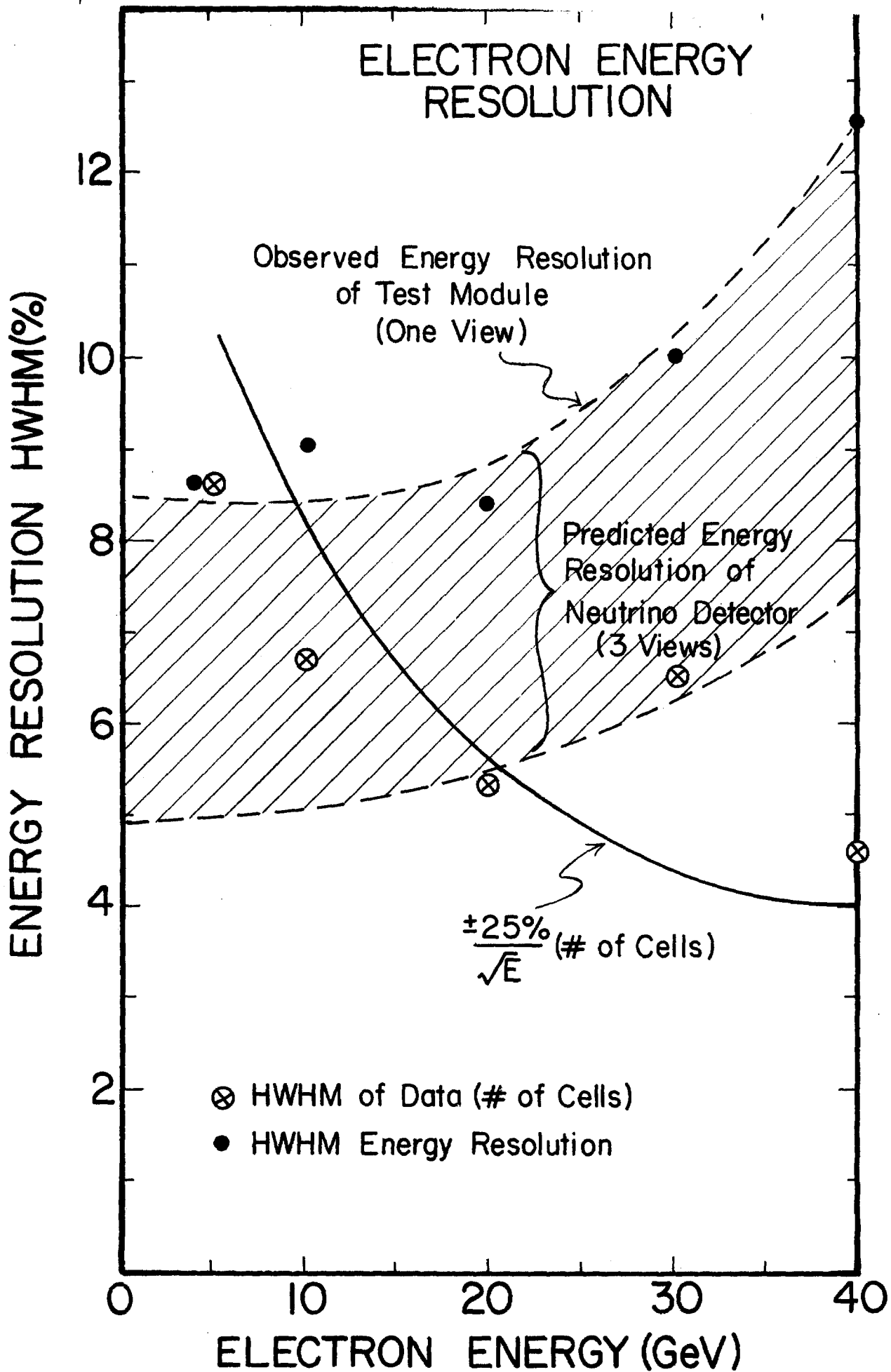


Fig A-5

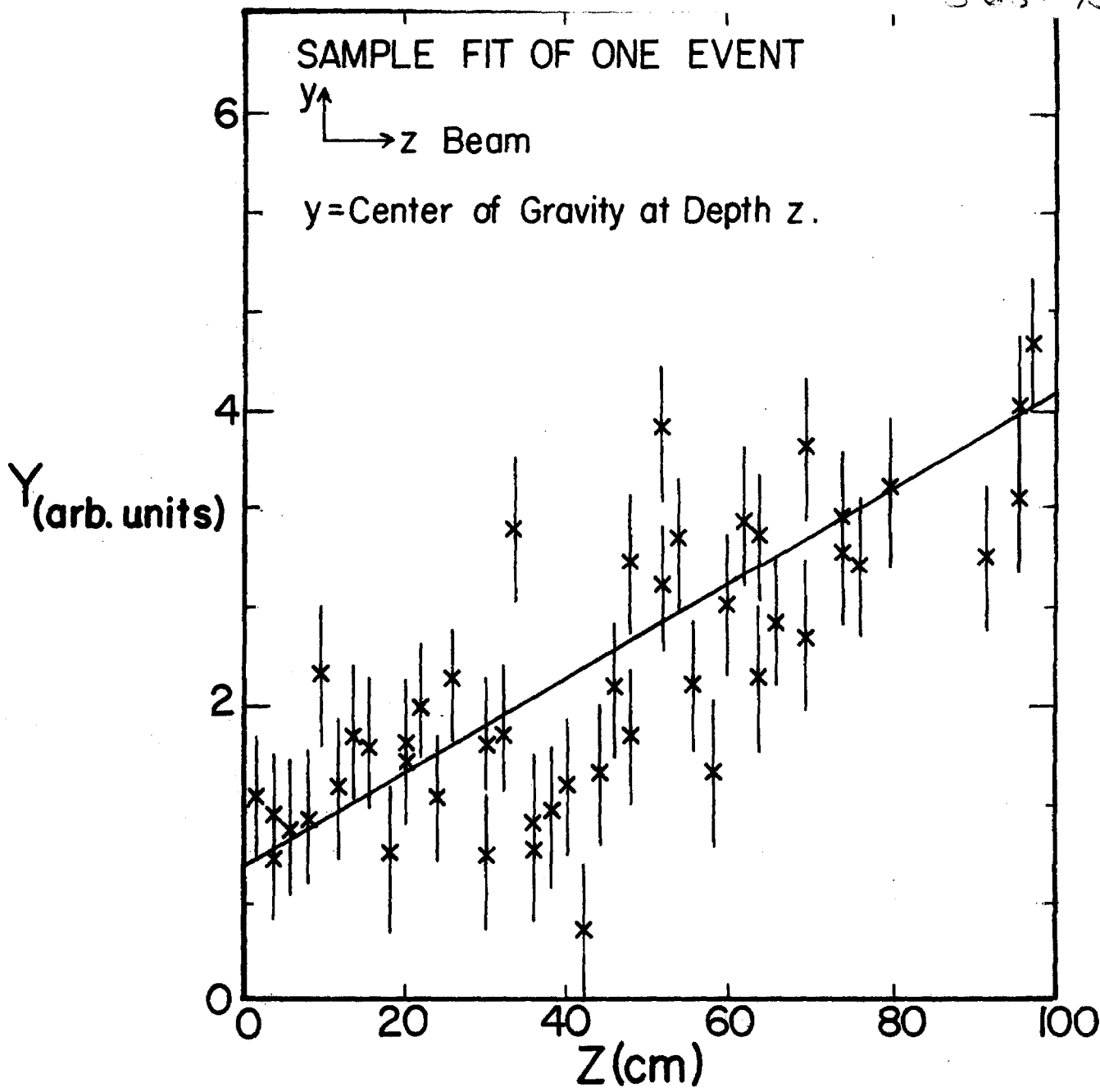


fig. A-6a

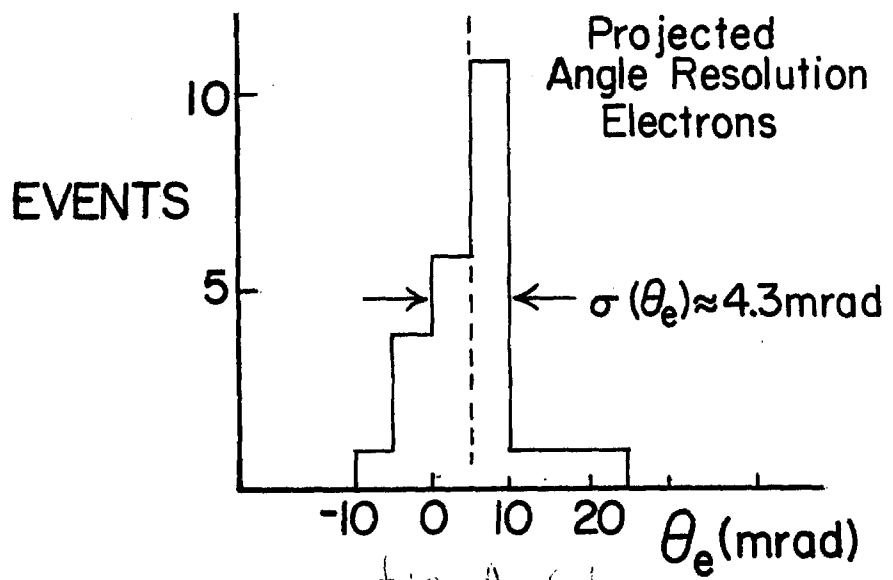


fig. A-6b

Hadron Shower Development

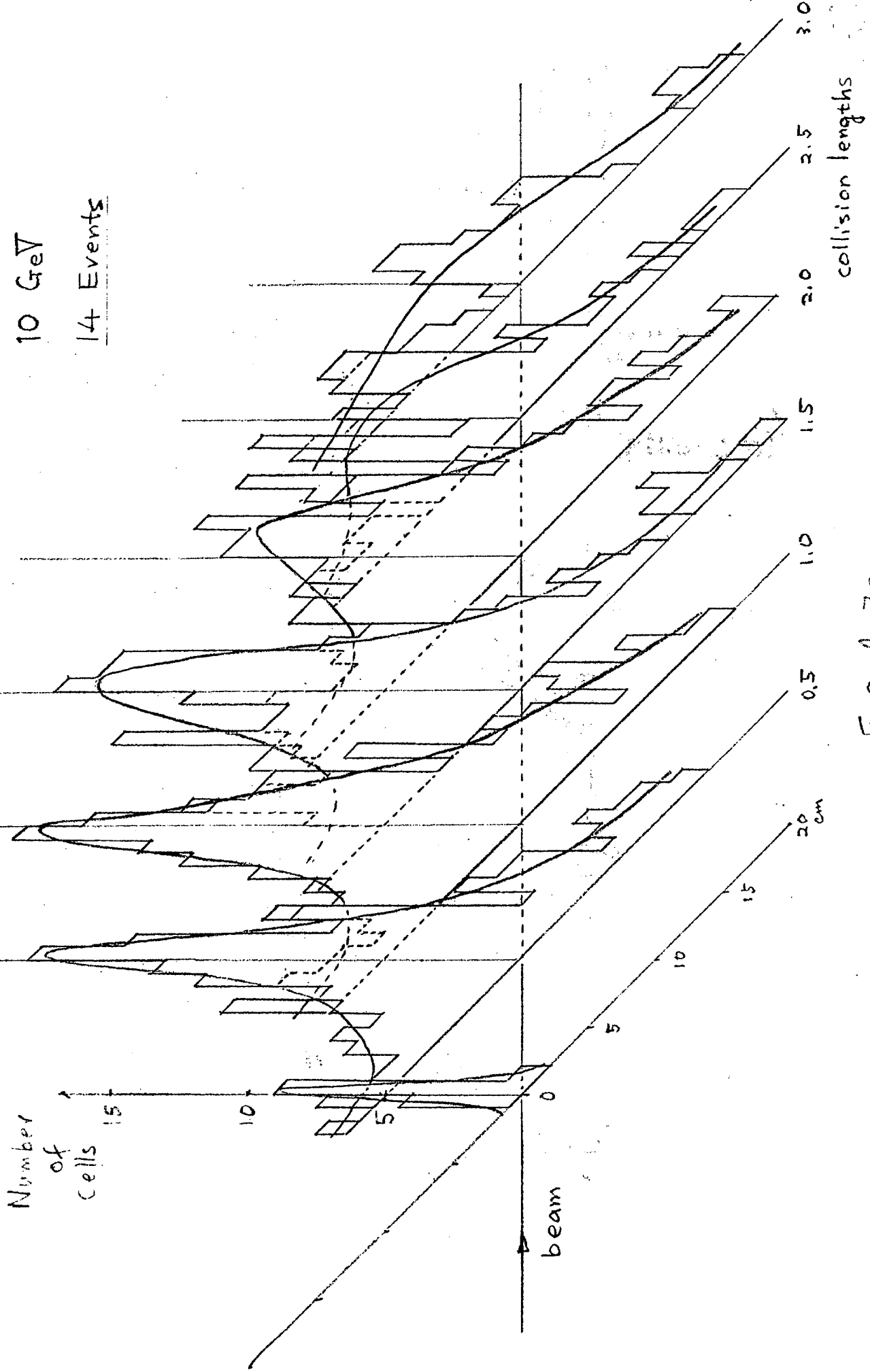


Fig A-7a

Hadron Shower Development

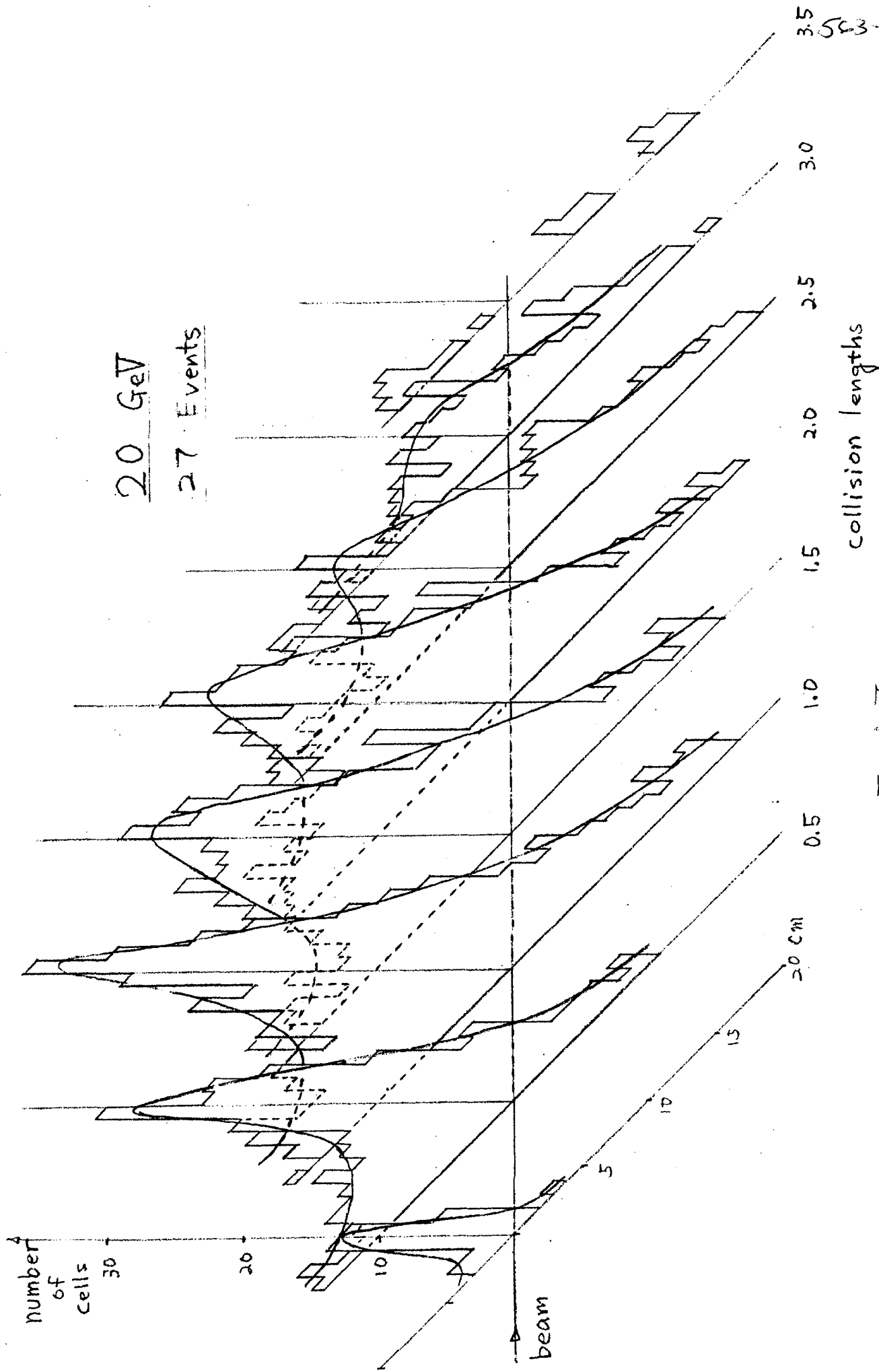


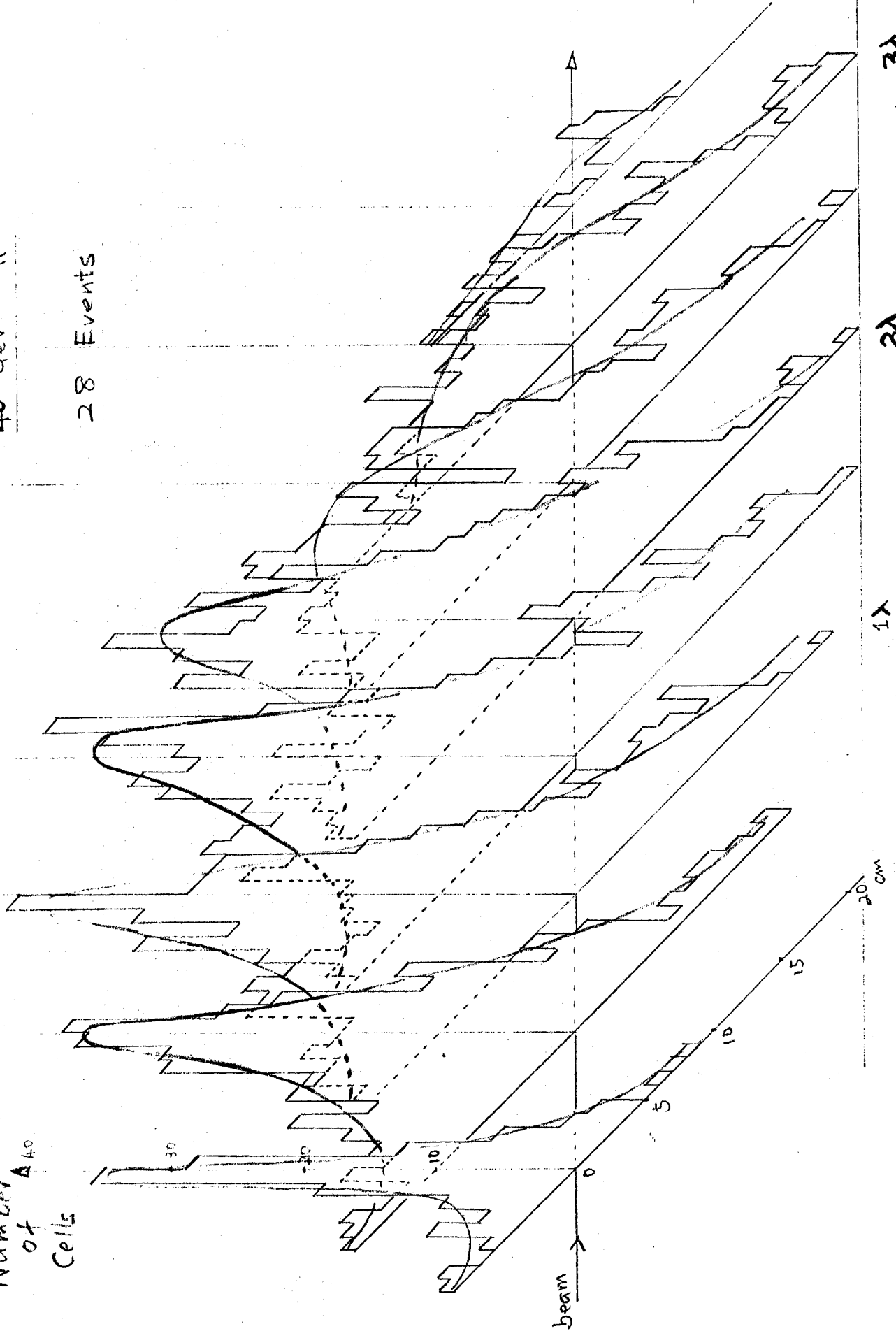
Fig. A-76

Hadron Shower Development

40 GeV π^+

28 Events

Number of Cells



3X

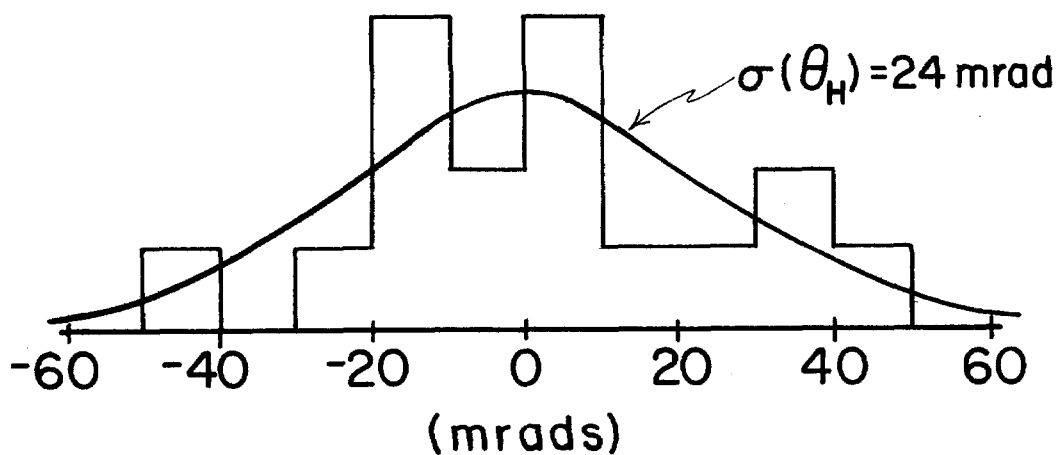
2X

1X

COLLISION LENGTHS

FIG. A-7C

ENERGY FLOW OF 20 GeV HADRONS



PROJECTED ANGLE DIST^N

FIG. A8

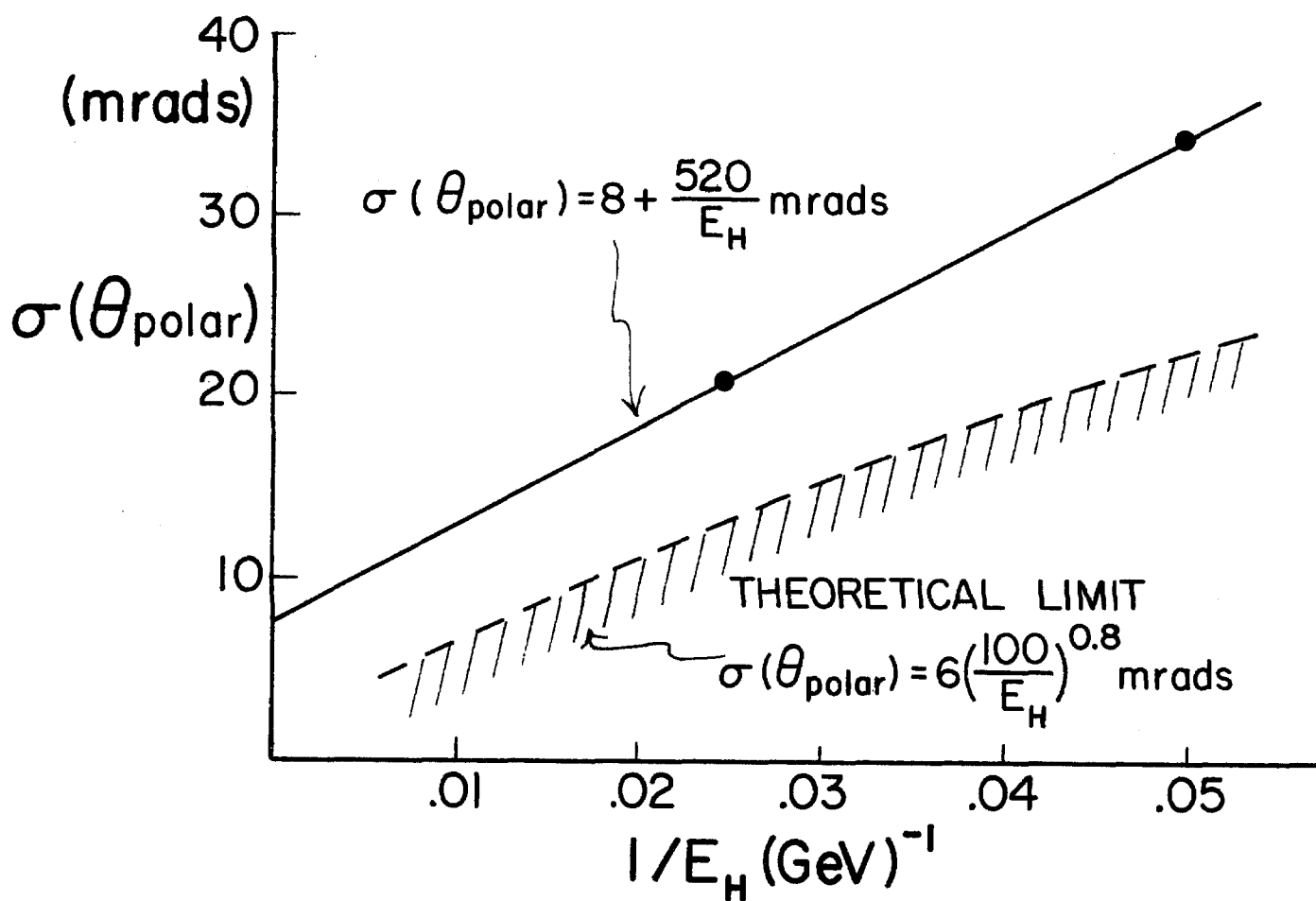
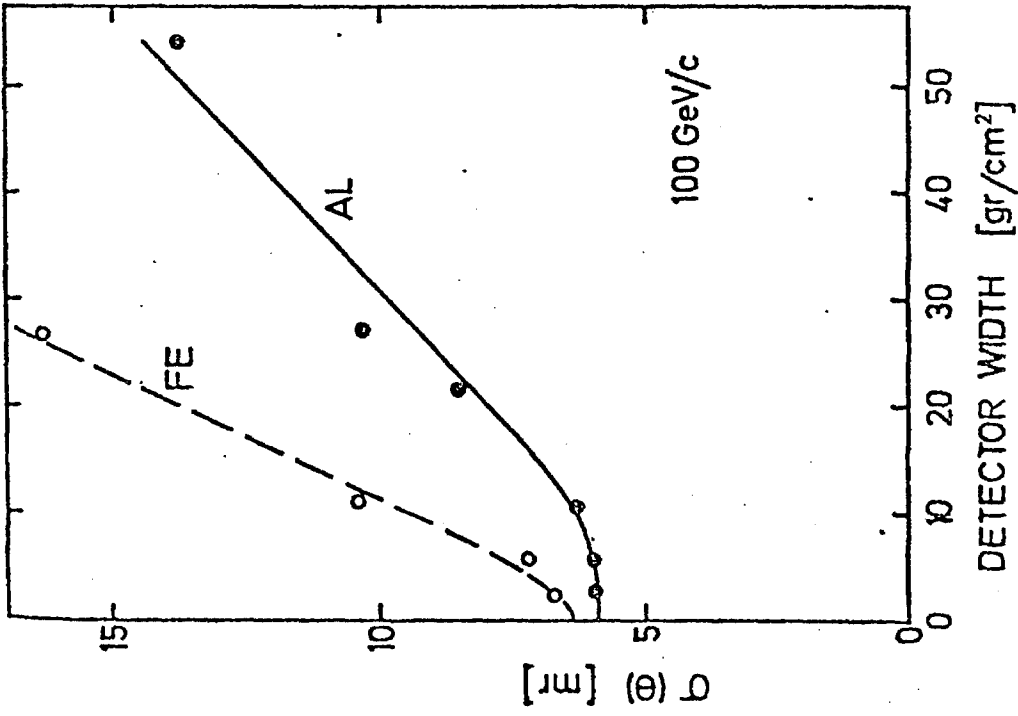
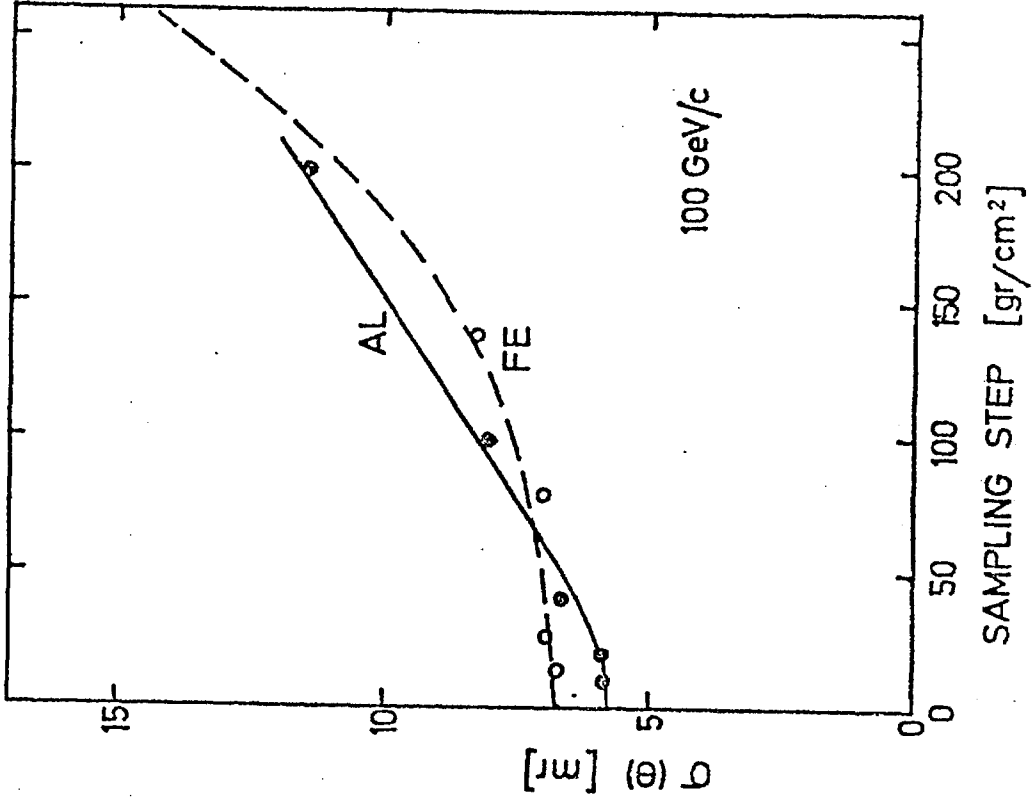


FIG. A9



(a)

Resolution $\sigma(\theta_H)$ on the hadron shower direction (assuming the apex position is known) as a function of the width of the detector elements, $\rho \cdot \Delta r$, for Al and Fe plates, where ρ is the average density ($E_H = 100 \text{ GeV}$).



(b)

Resolution $\sigma(\theta_H)$ on the hadron shower direction as a function of sampling step, $\rho \cdot \Delta t$ ($E_H = 100 \text{ GeV}$).

Fig. A10

APPENDIX B

ENGINEERING DESIGN STUDY OF 500 TON TARGET FABRICATION



SUBJECT

FLASH CHAMBER MODULES - J. WALKER et al.

NAME

W. Nestander

Cost and Production Studies - Preliminary Design

DATE

20 May 77

REVISION DATE

The purpose of this note is to investigate and summarize the production costs for a quantity of flash chamber modules, a new particle detector. These detectors are described in a draft proposal dated April 1977, by J. Walker et al. A detector module composed of 6 flash chambers, 5 filler sheets, and cover aluminum cover plates is investigated. (p.10)

Detector Tonnage

In the 65 lineal feet along the beam line that is considered available in Lab "C", a pattern of flash chamber modules, scintillation counters, and lead is used. (p.9). The total detector tonnage in this 65 ft. for the two types of detector fillers are: (lead and counters included)

<u>Type Modules</u>	<u>No. of Mod.</u>	<u>Wght. Mod.</u>	<u>Total Tonnage</u>
All 1/4" aluminum	204	4685#	571 tons
Alum. covers + 3/8" cement board.	172	4745	485 tons

Production Costs - Flash Chamber Modules

Material and labor costs for the two types of modules have been tabulated (p.3) and the quantities total as follows: (lead and counters not incl.)

All 1/4" aluminum	204	@	\$ 5,700	=	\$ 1,165 K
Alum. covers + 3/8" cement board	172	@	\$ 3,300	=	\$ 570 K

Production Time

Based on many "guesstimates" of design; production sequence, manpower and prototype development have been estimated (p. 4,5,6) Initial engineering development and prototype construction together with a pilot 10-module production run totals 7 months. After this point real production is:

<u>Type Module</u>	<u>Crew Size</u>	<u>No. to Make</u>	<u>Total Weeks</u>
All Aluminum	10 men	204	20 or 14 w/ O.T.
Alum Covers + 3/8" Cement Board	8	172	23 or 17 w/ O.T.

The overtime work assumes an 11 hour day with the same crew size to better use the facilities.

Facilities and Equipment

A shop area of 4000 square feet (32' x 125') has been planned for the production (p. 7,8) Tooling and equipment comes to \$ 55 K.

563-103

 FERMILAB ENGINEERING NOTE	SECTION	PROJECT	SERIAL-CATEGORY	PAGE
	Neutrino	Flash Ch.	77-511	3/1
SUBJECT			NAME	
FLASH CHAMBER MODULES - J. Walker et al.			W. Nestander	
Cost and Production Studies - Preliminary Design			DATE	REVISION DATE
			20 May 77	

SUMMARY - CEMENT BOARD MODULE TOTAL COSTS \$ / 1 module - 8 hr. day

<u>Item- Component</u>	<u>Mat. Cost</u>	<u>Prep. Labor</u>	<u>Assemb. Labor</u>
Aluminum Cover Plates (2 - 1/4")	\$ 1215	\$ 175	-
Aluminum Base & Lift Weldments	140	40	-
Flash Chamber Panels (6)	210	75	-
Gas Manifold Moldings (24)	40	90	-
Cement Board Fillers (5) - 3/8"	510	5	-
Aluminum Foil (2200 sf)	150	-	-
Epoxy Resins (6 gal.)	180	-	-
Insulation Blocks (5)	50	5	-
Module Lay-up & Assembly	-	-	\$ 340
	<u>\$ 2495</u>	<u>\$ 390</u>	<u>\$ 340</u>

TOTAL MODULE COST - CEMENT BOARD FILLER = \$ 3,300
 =====

SUMMARY - ALUMINUM PLATE MODULE TOTAL COSTS

Aluminum Cover Plates (2 - 1/4")	\$ 1215	\$ 175	-
Aluminum Base & Lift Weldments	140	40	-
Flash Chamber Panels (6)	210	75	-
Gas Manifold Moldings (24)	40	90	-
Aluminum Plate Fillers (5 - 1/4")	3035	220	-
Epoxy Resins (3 gal.)	90	-	-
Insulation Blocks (5)	50	-	-
Module Lay-up & Assembly	-	-	\$ 250
	<u>\$ 4780</u>	<u>\$ 600</u>	<u>\$ 250</u>

TOTAL MODULE COST - ALUMINUM PLATE FILLER = \$ 5,700
 =====